Clays and Clay Minerals, Vol. 60, No. 5, 507–534, 2012.

RIETVELD REFINEMENT OF DISORDERED ILLITE-SMECTITE MIXED-LAYER STRUCTURES BY A RECURSIVE ALGORITHM. I: ONE-DIMENSIONAL PATTERNS

KRISTIAN UFER[1,3]*, REINHARD KLEEBERG[1], JÖRG BERGMANN[2,†], AND REINER DOHRMANN[3]

[1] Institute of Mineralogy, TU Bergakademie Freiberg, Brennhausgasse 14, 09596 Freiberg, Germany
[2] Ludwig-Renn-Allee 14, 01217 Dresden, Germany
[3] BGR/LBEG, Stilleweg 2, 30655 Hannover, Germany

Abstract—X-ray diffraction patterns of oriented mounts of clay minerals are often used in clay mineralogy for qualitative and quantitative purposes. Fequently occurring stacking defects, in particular, can be characterized by this technique. Modeling of these diffraction profiles has become an important tool in obtaining structural information about the nature of stacking order. Manual matching of calculated and observed patterns is time consuming and user dependent. Automatic refinement procedures are, therefore, desirable. An improved approach for the treatment of disordered layer structures within a Rietveld refinement is presented here. The recursive calculation of structure factors, similar to that of the simulation program *DIFFaX*, was introduced in the Rietveld code *BGMN*. Complete implementation is formulated within the interpreter language of the Rietveld code and is transparent as well as flexible. Such a method has opened the application of Rietveld refinement to patterns of oriented mounts where only basal reflections of stacking disordered structures were recorded. The *DIFFaX* code was used to simulate basal reflections of illite-smectite mixed layers (I-S) with different ratios of illitic and smectitic layers and with different degrees of long-range ordering (Reichweite). Rietveld refinements with these simulated patterns were used to evaluate the application of this new approach. Several I-S with different degrees of ordering were also chosen as tests for the refinement of basal reflections. The samples were prepared as standard air-dried and ethylene glycol-solvated, oriented specimens. Realistic structural parameters were obtained for the composition and ordering of the I-S.

Key Words—*DIFFaX*, Illite-smectite, Rietveld Refinement, Stacking Faults.

INTRODUCTION

Minerals and synthetic substances with layered structures come in various forms with different degrees of stacking disorder owing to the weak interactions between adjacent layers. The stacking faults may consist of translational or rotational misorientation of layers, mixed layering of different layer types, or combinations of these. The diffraction patterns of such materials show strong anisotropic peak broadenings leading, in extreme cases, to modulated diffraction lines without reflections that may be indexed conventionally. These patterns are no longer describable by the traditional Bragg peak concept, thus precluding use of the standard Rietveld method in determining structural information or phase contents.

Layer silicates also show a strong tendency for preferred orientation due to their strong anisotropic crystallite shape. The classic Rietveld method normally uses data from powder diffraction measurements of unoriented or weakly oriented mounts. The effect of preferred orientation, normally avoided in powder diffraction, is used frequently in clay mineralogy for diagnostic or quantitative purposes. Layer silicates show similar lattice constants in the *a* and *b* directions, but clearly distinguishable diffraction features in the *c** direction. The typical preparation technique of the clay minerals as oriented mounts emphasizes the diagnostic basal reflections and suppresses the non-basal reflections. Several alternative software codes (*e.g. NEWMOD* (Reynolds, 1985), *MLM2C/3C* (Plançon and Drits, 2000), *MODXRD* (Plançon, 2004), and *NEWMOD+* (Yuan and Bish, 2010a)) are used to model basal reflections of such oriented mounts. Some programs contain automatic refinement routines (*e.g.* that by Plançon and Roux (2010), *SYBILLA* (by Aplin *et al.*, 2006), or *FITMOD* (by Yuan and Bish, 2010b)) and can handle mineral mixtures. The latter, therefore, provide quantitative information on phase contents. Such quantitative information is also influenced by the degree of preferred orientation of the individual minerals (*e.g.* Taylor and Norrish, 1966). Minerals in a mixture can, unfortunately, show different degrees of preferred orientation, which have to be corrected (*e.g.* Dohrmann *et al.*, 2009). Quantitative phase analysis based on modeling of basal reflections sometimes becomes inaccurate if the individual degree of preferred orientation of the minerals is unknown or is estimated inaccurately.

The aim of the present study was to demonstrate that the Rietveld method can be combined with a recursive

* E-mail address of corresponding author:
kristian.ufer@gmx.de
† Deceased
DOI: 10.1346/CCMN.2012.0600507

structure-factor calculation and, thus, is able to describe the diffraction of disordered stacking. The ability to fit basal patterns is described in this first paper (part I) and the limitations of the methods are discussed in part II (Ufer *et al*., 2012). The results (given here) are combined with a suitable description of the three-dimensional reflections (in part II) (Ufer *et al*., 2012). Development of models for qualitative and quantitative phase analysis with the Rietveld method, as already demonstrated for turbostratically disordered smectites (Ufer *et al*., 2004), is shown. In Ufer *et al.* (2008) the Rietveld method, combined with a recursive calculation of structure factors, was shown to be capable of refining structural models of stacking disordered, layered double hydroxides. The recursive calculation was developed by Treacy *et al.* (1991) and first implemented in the software code *DIFFaX*. The approach uses the self similarity of stacking sequences and allows the mathematical description of scattering by any layered structures in a set of simple equations. The original *DIFFaX* code was expanded (Leoni *et al.*, 2004; Casas-Cabanas *et al.*, 2006) by adding an automatic refinement procedure. Both programs (*DIFFaX+* and *FAULTS*) lack the option of dealing with mineral mixtures. This prevents application in quantitative phase analysis.

The structure-factor calculation as described by Treacy *et al.* (1991) was implemented in an existing Rietveld program instead of adding a refinement function to the original *DIFFaX* code (Ufer *et al.*, 2008). The full advantages of the *BGMN* software such as multiphase refinement and fundamental parameter approach could then be used. The aim of the present study was to examine the reliability of this approach for the refinement of structural features of disordered layered structures.

Illite-smectite mixed-layered minerals are the most common and arguably the most important clay minerals for the study of diagenetic processes. Accurate structural and phase analysis poses a significant challenge in the daily work of mineralogical laboratories. In general, illite-smectites are fine-grained, dioctahedral, 2:1 phyllosilicates. The 2:1 phyllosilicates consist of two corner-sharing tetrahedral sheets which sandwich an octahedral sheet.

The stacking sequences of illitic and smectitic layers are often disordered and can only be described statistically with different degrees of long-range ordering (Reichweite or R). The term Reichweite, as defined by Jagodzinski (1949), describes the extent of the dependency of the occurrence of a given layer on the nature of its adjacent layers.

The coexistence of smectitic interlayers in different hydration states also leads to a stacking of smectitic layers with different basal spacings. Both effects, the disordered stacking of illitic and smectitic layers, and the inhomogeneous hydration of the interlayer cations, lead to a non-rational series of the basal reflections.

In this first part of the study, the refinement of simulated and observed data of several I-S minerals with different degrees of disorder is demonstrated. No attempt was made to quantify mixtures, but the correct description of the 00*l* reflections is needed for the Rietveld refinement of powder patterns which is demonstrated in part II (Ufer *et al.*, 2012).

RECURSIVE CALCULATION OF STRUCTURE FACTORS AND DIFFRACTION INTENSITIES

The recursive description of diffraction from an infinite stack of n layer types, as described by Treacy *et al.* (1991, 1993), results in a set of simple equations (1):

$$\mathbf{\Psi} = \mathbf{F} + \mathbf{T} \cdot \mathbf{\Psi} \quad (1)$$

or, as an equation system, *e.g.* with three different layer types:

$$\Psi_1 = F_1 + T_{11} \cdot \Psi_1 + T_{12} \cdot \Psi_2 + T_{13} \cdot \Psi_3$$
$$\Psi_2 = F_2 + T_{21} \cdot \Psi_1 + T_{22} \cdot \Psi_2 + T_{23} \cdot \Psi_3$$
$$\Psi_3 = F_3 + T_{31} \cdot \Psi_1 + T_{32} \cdot \Psi_2 + T_{33} \cdot \Psi_3$$

The array **F** contains the structure factors F_i of all n layer structures. **Ψ** is the scattered wavefunction at a given reciprocal lattice point *hkl*. **T** contains the translational vector t_x,t_y,t_z in relative coordinates of the given lattice from a layer i to layer j and its components are defined as (2):

$$T_{ij} = p_{ij} \cdot \exp(-2 \cdot \pi \cdot i \cdot (h \cdot t_x + k \cdot t_y + l \cdot t_z)) \quad (2)$$

p_{ij} is the probability that one layer j follows one layer i. The complex coefficients of **T**, **F**, and **Ψ** are handled in component notation (real and imaginary parts) in the present study to allow summations.

The structure factor, F, is calculated from the structures of the given layer types with these layers taken as infinite in the a and b directions. The components of the complex matrix **T** are calculated within two nested loops in *BGMN*, while the equation system is solved with a built-in solver function. Equation 1 is transformed to a regular equation 3:

$$\mathbf{F} = \mathbf{\Psi} - \mathbf{T} \cdot \mathbf{\Psi} = \mathbf{\Psi} \cdot (\mathbf{E} - \mathbf{T}) \quad (3)$$

or as an equation system:

$$F_1 = \Psi_1 \cdot (1 - T_{11}) - \Psi_2 \cdot T_{12} - \Psi_3 \cdot T_{13}$$
$$F_2 = -\Psi_1 \cdot T_{21} + \Psi_2 \cdot (1 - T_{22}) - \Psi_3 \cdot T_{23}$$
$$F_3 = -\Psi_1 \cdot T_{31} - \Psi_2 \cdot T_{32} + \Psi_3 \cdot (1 - T_{33})$$

E is the unit matrix. The overall structure factor is calculated as the incoherent sum of the weighted coefficients of **Ψ**. The weighting factor w is the *a priori* probability that a layer i exists in the stack and is calculated as:

$$w_i = \sum_j w_j \cdot p_{ji} \quad (4)$$

https://doi.org/10.1346/CCMN.2012.0600507 Published online by Cambridge University Press

using the boundary conditions that the sum of all proportions w_i is equal to one and that the sum of all stacking probabilities from a layer i (p_{ij} over j) is also equal to one.

DESCRIPTION OF LONG-RANGE ORDERING BY THE REICHWEITE CONCEPT

The stacking sequences of a disordered I-S can only be described statistically with different long-range ordering (Reichweite). The term Reichweite, as defined by Jagodzinski (1949), describes the extent of influence on the probability of the occurrence of a layer. A Reichweite value of R3, for example, means that layers up to the third next neighbor have to be considered to specify the nature of the 'next' layer. Jagodzinski (1949) described Reichweite values for SiC up to R6. Only values R0 to R3 are reported in the literature for I-S minerals. The definition of junction probabilities p and proportions w of layers, layer pairs, and triple layer stacks is necessary for a quantitative description of the one-dimensional structure of a mixed-layer mineral. A set of independent probability parameters has to be chosen for each Reichweite value. The dependencies of all other parameters can be related to each other by linear equation systems. The choice of these independent parameters is not unique and certain assumptions can be drawn for I-S stacks. Because of this, all equations used in the present work are described in detail although other comprehensive descriptions already exist (Reynolds, 1980; Drits and Tchoubar, 1990).

The following boundary conditions for deduction of the dependencies exist. First, the sum of all proportions of layer kinds is equal to one. Second, the sum of all probabilities for the occurrence of the following kind of layer is also one. In addition, all values are constrained to the range zero to one, because negative proportions/probabilities or values greater than one physically make no sense. The sum of the proportion of illitic layers and smectitic layers in an I-S is one:

$$wI + wS = 1 \quad (5)$$

wI is chosen as a refineable parameter in all models and wS is calculated as

$$wS = 1 - wI \quad (6)$$

All junction probabilities can be derived from wI in the case of random interstratification (R0). pII, the probability that an illitic layer follows another one is equal to the probability that I follows S and simply depends on the proportion of I:

$$pII = pSI = wI \quad (7)$$

The boundary conditions lead to:

$$pIS = 1 - pII \quad (8)$$

and

$$pSS = 1 - pSI \quad (9)$$

Only one statistical parameter (wI) has to be refined to describe an R0 disordered stacking. Equations 5, 6, 8, and 9 are valid for all degrees of Reichweite for two-component mixed layers.

Equation 7 is no longer generally valid in the case of R1, and pII must be declared as an independent and refineable variable. The proportion of I can be calculated by applying equation 4. wI is equal to the probability that I follows another I multiplied by the proportion of I plus the probability that I follows S multiplied by the proportion of S:

$$wI = wI \cdot pII + wS \cdot pSI \quad (10)$$

pSI can be calculated after rearranging:

$$pSI = (wI - wI \cdot pII)/wS \quad (11)$$

or

$$pSI = wI \cdot (1 - pII)/(1 - wI) \quad (12)$$

pIS and pSS are determined according to equations 8 and 9.

Some combinations of these two independent variables, wI and pII, are forbidden. pSI cannot become negative because the term $wI \cdot (1 - pII)$ in equation 12 is always the product of two positive values and $1 - wI$ is also always positive. pSI can become >1 for some combinations of wI and pII, though. The maximum value allowed for pSI is one. In this case, $pSS = 1 - pSI = 0$ describes the situation that a smectitic layer never follows another smectitic layer. This refers to the maximum possible degree of ordering (mpdo). The mpdo condition is only possible for wI values >0.5. The following relationship of pII and wI can be deduced, putting the mpdo condition pSI = 1 in equation 12 and rearranging:

$$pII\ (mpdo) = (2wI - 1)/wI \quad (13)$$

pII values smaller than pII (mpdo) are not permitted for wI >0.5. The Rietveld software *BGMN* allows refinement of parameters with dynamic limits. The lower limit of pII is zero (for $wI < 0.5$) or pII (mpdo) (for $wI \geqslant 0.5$).

The conditions for the maximum possible degree of ordering do not need to be present in R1 ordered stacks. The assumption, though, that IS stacks with greater degrees of long-range ordering (R2 and R3) show mpdo ordering for R1 parameters seems to be valid in most I-S minerals (Bethke *et al.*, 1986).

Such recursive treatment requires the definition of layer pairs to describe R2 ordering because stacking sequences are not defined explicitly. Four different pairs are possible: II, IS, SI, and SS. SS stacks are not present (wSS = 0) if R1 (mpdo) is assumed. The other layer pair proportions can be calculated using the previously defined or deduced parameters:

$$wII = wI \cdot pII \quad (14)$$

https://doi.org/10.1346/CCMN.2012.0600507 Published online by Cambridge University Press

$$wIS = wI \cdot pIS \quad (15)$$
$$wSI = wS \cdot pSI \quad (16)$$

The following probabilities have to be considered for R2 ordering: *p*III, *p*IIS, *p*ISI, *p*ISS, *p*SII, *p*SIS, *p*SSI, and *p*SSS. *p*SSS and *p*SSI do not need to be considered. One of these conditional probabilities or even both may be greater than zero but they are redundant because the *a priori* condition that an SS pair exists is zero. *p*ISS is also zero because of the R1 (mpdo) condition and, due to this, *p*ISI is equal to one. *p*III is chosen as an independent and refineable parameter in this work. *p*IIS is equal to 1 − *p*III. *p*SIS depends on *p*IIS analogous to equation 10:

$$wIS = wII \cdot pIIS + wSI \cdot pSIS \quad (17)$$

or rearranged:

$$pSIS = (wIS - wII \cdot pIIS)/wSI \quad (18)$$

*p*SII is equal to 1 − *p*SIS.

The maximum possible degree of ordering is derived in R2 ordered stackings for *p*SIS = 0. Analogous to equation 17, *w*II can be described as:

$$wII = wII \cdot pIII + wSI \cdot pSII \quad (19)$$

or rearranged:

$$pIII = (wII - wSI \cdot pSII)/wII \quad (20)$$

In the case of R2 (mpdo), *p*III is no longer independent and can be described by equation 21, using equations 13 and 16 and the mpdo conditions:

$$pIII\ (mpdo) = (3wI - 2)/(2wI - 1) \quad (21)$$

R2 (mpdo) is only defined for *w*I values >2/3. R2 ordering without the condition of mpdo is defined for *w*I $\geqslant$ 0.5, because the assumption R1 (mpdo) does not allow *w*I < 0.5. *p*III can be refined with a dynamic limit which is zero for 0.5 < *w*I < 2/3 and *p*III (mpdo) for *w*I $\geqslant$ 2/3.

Triple layer stacks have to be defined to describe R3 ordering. The assumption of R1 (mpdo) and R2 (mpdo) reduces the number of triple stacks to four: III, IIS, ISI, and SII. Their proportions are:

$$wIII = wII \cdot pIII \quad (22)$$
$$wIIS = wII \cdot pIIS \quad (23)$$
$$wISI = wIS \cdot pISI \quad (24)$$
$$wSII = wSI \cdot pSII \quad (25)$$

mpdo also reduces the number of junction probabilities which have to be defined to describe the probability that a layer follows a triple layer stack. *p*IIII is chosen as a refineable variable. *p*IIIS is 1 − *p*IIII. *p*SIII can be calculated from *p*IIII using equation 26:

$$wIII = wIII \cdot pIIII + wSII \cdot pSIII \quad (26)$$

or rearranged:

$$pSIII = (wIII - wIII \cdot pIIII)/wSII \quad (27)$$

*p*SIIS is equal to 1 − *p*SIII. *p*IISS is equal to zero, because R1 (mpdo) requires that S never follows S. *p*IISI is equal to one. *p*ISII is calculated by equation 28:

$$wSII = wISI \cdot pISII + wSSI \cdot pSSII \quad (28)$$

*w*SSI is equal to zero and *p*ISII = *w*SII/*w*ISI.

R3 ordering shows the maximum possible degree of ordering for *p*SIII = 1. This leads to equation 29:

$$pIIII\ (mpdo) = (4wI - 3)/(3wI - 2) \quad (29)$$

R3 (mpdo) is only possible for *w*I $\geqslant$ 0.75. *p*IIII (mpdo) is the lower dynamic limit for a refinement of *p*IIII in this range. The limit is zero for 0.67 < *w*I < 0.75.

All models developed in this work use the statistical description for stacking of two layer types. But the smectite interlayer space exists in the two different hydration states for all Reichweite values (monohydrated '1w' and bihydrated '2w'). These two different hydration states coexist and can be transferred into each other by changing the environmental relative humidity. This system is not regarded here as a three-layer stacking, but as a two-layer system with an additional probability parameter *p*1w which defines whether the 1w or the 2w type occurs. The limitation to a random distribution of 1w and 2w hydrated smectitic interlayers seems to be justified for the illite-dominated minerals in this study.

MATERIALS AND METHODS

The present study can be divided into two parts. First, diffraction patterns of three different I-S minerals were calculated with the simulation software *DIFFaX* and then fitted with the Rietveld software *BGMN*. The use of calculated data allows a more in-depth evaluation of the refinement results than the use of measured data. The strategy of applying four different models for the refinements was chosen to evaluate the performance of the automatic routine. The chosen strategy is not the only one which leads to a result and the choice of how best to apply this tool depends on the user and the topic. The description of the three examples gives a better understanding of the sensitivity and significance of the different adjustable parameters.

Second, the structure models were applied to refine observed data of three I-S. The same 'user-independent' refinement strategy (starting from different models) as before was applied and the outcome of the previous refinements was considered in discussing the results.

Simulation by DIFFaX

DIFFaX is well established and has led to reliable results in numerous applications. The results of *DIFFaX* calculations and *BGMN* calculations with the same structural parameters lead to almost identical results (Ufer *et al.*, 2008), because both programs use the same mathematical description of the diffraction process.

https://doi.org/10.1346/CCMN.2012.0600507 Published online by Cambridge University Press

Small deviations are probably the result of individual precision or the design of numeric routines of the two programs. The simulated data in the present work covers a range of different ratios from illite to smectite and different degrees of ordering. The input data were chosen to reflect natural materials although simplifications were made.

The atomic Z coordinates of the TOT layers were derived from Drits *et al.* (2006) (Table 1). The original values were recalculated for an orthogonal unit cell with the basal oxygen at $Z = 0.000$ Å. The atomic positions of the symmetrically equivalent positions were calculated considering the two-fold axis of the TOT layers. Typical values were chosen for the occupancies. The interlayer cation Ca for both hydration states was placed on the interlayer midplane with an occupancy of 0.2. The water molecules of the 1w state (represented only by oxygen atoms) are also on the midplane with four times greater occupancy to describe a square planar coordination. Two planes of three oxygen atoms per Ca were placed 1.2 Å below and above the cation for the bihydrated state (Ferrage *et al.*, 2005b). Both positions have occupancy which is three times greater than the Ca. This arrangement reflects the projection of an octahedral coordination of the interlayer cation with two triangles of the octahedron parallel to the TOT layers.

The structure of the ethylene glycol (EG) molecule is derived from Oie *et al.* (1994). Two of these molecules were placed in the interlayer so that their symmetry plane lies perpendicular to the TOT layer (Figure 1). The two molecules were placed symmetrically to the midplane, so that they have the same distance *d*(EG) to the TOT layer, one to the underlying and one to the following. In addition, two Ca positions and two layers of water were added in the EG-solvated interlayer. The positions were also defined by their distance to the midplane, $d(Ca,H_2O)$. The Debye-Waller factor of all atoms was set to zero.

The repeating distance in the *c* direction for the illitic layers was set to 9.99 Å. The smectitic repeating distances for the monohydrated (1w) and bihydrated (2w) air-dried (AD) state were set to 12.5 Å and 15 Å. 16.8 Å was used for EG-intercalated material.

The *DIFFaX* calculations were performed for a monochromatic wavelength of 1.789007 Å ($CoK\alpha_1$) and a Lorentzian-shaped instrumental broadening with a constant full-width at half-maximum intensity of 0.6º. The resulting intensities were converted from a fixed divergence slit measurement (I_{fix}) to a measurement with variable divergence slit and constant irradiated sample length (I_{var}) by the relation $I_{var} = I_{fix} \cdot \sin\theta$. The *DIFFaX* calculations show a strong intensity decay at the beginning of the calculation range (Figure 2). This artifact could be eliminated by choosing a larger simulation range than the intended refinement range. Refinements were performed over the range 2–65º2θ, while the simulation started at 1º2θ and ended at 80º2θ. *BGMN* also showed a decay at the lower end of the refinement because *BGMN* produces the continuous diffraction line by overlapping of numerous peaks and the intensities at the beginning of the refinement range should be produced from peaks just under the lower range limit. Unfortunately *BGMN* cannot generate peaks outside the refinement range but the lack of intensity was compensated by an increase in the background line.

The three simulated patterns were generated for an R0 disordered I-S (wI = 0.25), an R1 ordered I-S (wI = 0.5), and an R3 ordered I-S (wI = 0.9). The complete statistical parameters are reported in the tables of the results section for a direct comparison of input data and refinement results.

Background intensities and instrumental noise were added to the simulated intensities. These two contributions were extracted from observed data of a well crystalline material (quartz).

Table 1. Structural parameters for the *DIFFaX* simulations of I-S diffraction patterns.

Repeating distance	
Layer type	t (Å)
Illitic	9.99
Smectitic (1w)	12.50
Smectitic (2w)	15.00
Smectitic (EG)	16.80

Atomic positions and occupancies

Atom	Z (Å)	Occupancy p
Illitic TOT layer		
Si	0.656	0.9
^{IV}Al	0.656	0.1
Fe	3.350	0.1
Mg	3.350	0.3
Al	3.350	0.6
O1	2.273	1.0
O2	0.217	1.0
O3	0.000	1.0
OH	2.347	1.0
Illitic interlayer		
K	8.345	0.8
Smectitic interlayer		
Ca	midplane	0.2
H_2O (1w)	midplane	0.2×4
H_2O (2w)	midplane ± $d(H_2O)$	0.2×3
$d(H_2O)$	1.2	
EG intercalated interlayer		
Ca	midplane ± $d(Ca,H_2O)$	0.1
H_2O	midplane ± $d(Ca,H_2O)$	0.1
EG molecules	midplane ± d(EG)	1.0
$d(Ca,H_2O)$	2.525	
d(EG)	2.150	
h(EG)	0.867	

https://doi.org/10.1346/CCMN.2012.0600507 Published online by Cambridge University Press

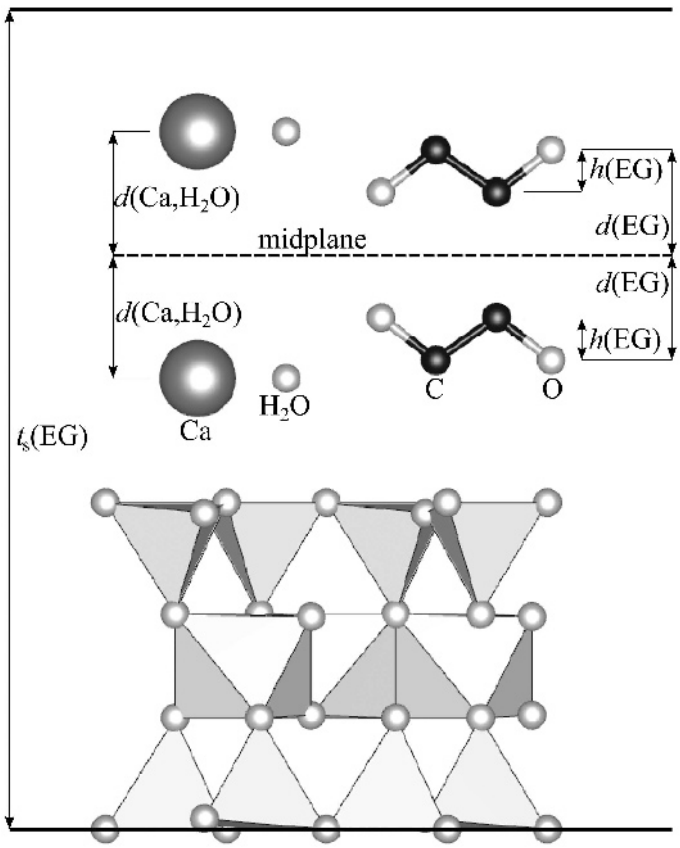

Figure 1. Structure of an EG-intercalated smectitic layer.

Rietveld refinements of simulated data

The Rietveld software *BGMN* (Bergmann *et al.*, 1998) was used for the recursive calculations inside a Rietveld refinement. *BGMN* contains an interpreter language which allows the definition of additional functions and parameters. The manipulation of the complex structure factors of multiple layer structures within a single unit cell, the so-called sub-phases, is also possible. The use of an interpreter language allows a very flexible and transparent formulation without the necessity of hard coding. A super-cell approach was used to calculate the structure factors of these sub-phases periodically in the *a* and *b* directions and aperiodically in the *c* direction. Such an approach was proposed by Ufer *et al.* (2004) to treat turbostratic disorder. Diffraction by a turbostratic structure is equivalent to diffraction by a single layer with respect to non-basal reflections. The use of an elongated and less than half filled unit cell for structure-factor calculation approximates the Fourier transformation of an aperiodic object, which is the mathematical interpretation of the diffraction process on a single layer. In contrast, the stacking of illitic and smectitic layers in the *c** direction was introduced here by the recursive calculation. The super-cell was enlarged by a factor of 100 in the *c** direction and only partly filled with one layer (R0 and R1), one layer pair (R2), or one layer triplet (R3) per sub-phase. This approach provides enough sampling points in the reciprocal space and peak positions in the

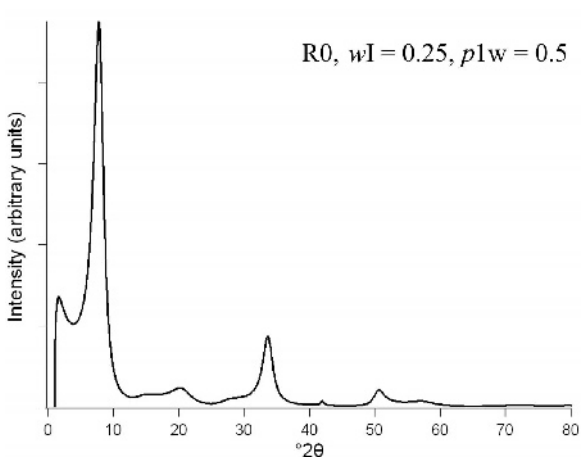

Figure 2. Simulated pattern of an R0 ordered I-S using the parameters in Tables 1 and 3. Raw data without background and instrumental noise, converted for variable divergence slits.

https://doi.org/10.1346/CCMN.2012.0600507 Published online by Cambridge University Press

powder pattern to produce a quasi continuous run of the diffraction pattern.

Some extra functions were introduced in addition to the structure-factor calculation. The recursive treatment regards a stack as infinite and in the case of ordered stacking, a reflection becomes infinitely sharp though still having a finite area. This effect is problematic for a correct numerical integration when the stacking is only slightly disordered. An additional function was added to ensure a minimal integrable width of all reflections. A function for the calculation of correct densities from the partly filled unit cell and for a constant Lorentzian-shaped peak broadening was also introduced.

Several refinements for each data set were performed with different models and refineable parameters. These parameters can be divided into two groups. One mainly affects the position of the intensity maxima, and the other affects the intensity distribution. The first group contains the translations within the layer plane and perpendicular to it, the proportions, and the probabilities. The second one contains the occupancies and positions of the atoms in the unit cell.

The refinement strategy of the simulated patterns described here reflects a situation in which the only known fact is that the smectitic interlayers are intercalated with hydrated Ca ions (or EG molecules in the third example). No other information may be available initially. A first 'trial-and-error' step to identify the nature of the stacking was a refinement with all four I-S models (R0 to R3), using intermediate starting parameters. Chemical information was assumed in a further step to fix the occupancies. The structural parameters which were used for the refinements were mainly identical to those used in the simulations. The repeating distance c for the illitic layers was kept fixed. The smectite repeating distances for the mono- and bihydrated AD state were refined between limits taken from Ferrage *et al.* (2005a), and from Ferrage *et al.* (2007) for the EG-solvated state. The positions of the atoms in the TOT layer were kept fixed. No attempt was made to refine the ratio of Si and Al in the tetrahedral positions, due to their similar scattering power. The Mg occupancy in the octahedral position was kept fixed, the Fe occupation was refined and the Al occupation was, therefore, calculated as $p(\mathrm{Al}) = 1 - p(\mathrm{Mg}) - p(\mathrm{Fe})$. The occupancies of the interlayer cations in the AD state, of the EG molecules, and of the interlayer water molecules were refined. The occupancy of Ca in the EG-intercalated state was fixed to 0.1 due to its small content in relation to the EG content. The positions of the interlayer cations were formulated in relation to the repeating distance to ensure that the cations were always on the midplane or, in the case of EG and bihydrated states, symmetrical to the midplane. The distances from the water molecules in the 2w state and the EG molecules to the midplane were refined. The starting values for the proportions of layer types were set to an intermediate value with refinement limits related to the actual degree of Reichweite. All starting parameters and refinement limits are declared in the corresponding tables in the Results section.

A scaling factor and a constant peak broadening factor were refined. The background was described by a Lagrange polynomial of 6th degree. The strict monochromatic wavelength of the simulations (1.789007 Å) was also used in the refinements.

Rietveld refinements of observed data

The starting structural parameters of the models for the refinement of observed data were nearly the same as in the refinements of the simulated data. The Debye-Waller factor was set to 1 Å^2. The atomic positions of the glauconitic TOT layer were changed according to Sakharov *et al.* (1990) (Table 2). The layer-to-layer distance c for the glauconitic layers was set to 9.94 Å. The first refinement tests showed that the refinement of the number of interlayer water and EG molecules nearly always reached the upper limit. This limit was increased to 3 per water layer for the interlayer water of the smectitic layers and 2 per water layer and EG molecule for the EG-intercalated state.

The following conditions were chosen for the Rietveld refinements in addition to the structural specific parameters. *BGMN* includes a fundamental parameter approach to model the instrumental part of the peak profile (Cheary and Coelho, 1992). The instrument-dependent part of the diffraction profile was determined by a ray-tracing procedure prior to the refinement. The zero point, the sample displacement error, and a Lagrange polynomial of 6th degree for the description of the background were refined as non-structural parameters.

Table 2. Structural parameters for the refinements of G-S diffraction patterns. All other parameters are identical to the I-S structural parameters (Table 1).

Repeating distance	
Layer type	t (Å)
Glauconitic	9.94
Atomic positions	

Atom	Z (Å)
Glauconitic TOT layer	
Si	0.630
^{IV}Al	0.630
Fe	3.350
Mg	3.350
Al	3.350
O1	2.250
O2	0.110
O3	0.000
OH	2.280
Glauconitic interlayer	
K	8.320

https://doi.org/10.1346/CCMN.2012.0600507 Published online by Cambridge University Press

Characterization of sample materials

The insight which emerged from the refinement of simulated data was applied to the evaluation of the refinement results of observed data. Three materials with different degrees of ordering were chosen as test materials. All samples were also characterized by X-ray fluorescence (XRF) to evaluate the occupancies.

The sample referred to as Urkut is a glauconitic material collected in the area of a manganese deposit near Urkut, Hungary. The assumption was made here that the disorder in glauconite-smectite (G-S) is equivalent to that of I-S and the statistical description of I-S stacks can be transferred to G-S stacks.

The sample ISCz-1 is a clay mineral from Slovakia and a Special Clay from the Source Clays Repository of The Clay Minerals Society (CMS). It is described as an ordered I-S with an illite:smectite ratio of 70:30. The reference formula from the CMS website (http://www.clays.org/SOURCE%20CLAYS/SCdata.html) is

$$Mg_{0.015}Ca_{0.05}Na_{0.045}K_{0.475}Si_{3.59}Al_{0.41}(Al_{1.70}Fe^{3+}_{0.06}Mg_{0.24})O_{10}(OH)_2.$$

The following formula was reported by Gailhanou *et al.* (2007):

$$K_{0.530}Na_{0.135}Si_{3.565}Al_{0.435}(Al_{1.709}Fe^{3+}_{0.051}Mg_{0.218}Fe^{2+}_{0.017}Ti_{0.005})O_{10}(OH)_2.$$

Sample F4 is a dioctahedral illite-smectite mixed-layer mineral collected from the Korom Hill deposit near Füzérradvány, close to Satoraljaújhely, northern Hungary. The material from this deposit was originally described as a "sarospatakite" comparable to "illite" (Maegdefrau and Hofmann, 1937) and further characterized more recently (*e.g.* Ahn and Buseck, 1990; Środoń *et al.*, 1992; Gualtieri *et al.*, 2008).

Material pretreatment

All samples were size fractionated in the gravity field (Atterberg method) in order to reduce the amount of quartz and other impurities. All clay minerals were Ca saturated after the collection of the <2 μm fractions. Excess salt was removed by dialysis using deionized water. Traces of quartz were still present in the clay fractions, as well as some kaolinite in sample ISCz-1.

Chemical analysis (XRF)

The chemical composition of powdered samples was analyzed using a PANalytical Axios and a PW2400 XRF spectrometers. Samples were prepared by mixing with a flux material and melting into glass beads. The beads were analyzed by wavelength dispersive XRF spectrometry (WD-XRF). 1 g of sample material was heated to 1030ºC for 10 min to determine loss on ignition (LOI).

The XRF data were used to develop a structural formula following the procedure of Marshall (1935, 1949) and Ross and Hendricks (1945). Quartz amounts of 10 wt.% for the Urkut sample, 2 wt.% for ISCz-1, and 4 wt.% for F4 were considered. These values result from estimations with Rietveld refinements using approximate ideal structural models. The kaolinite content of ISCz-1 was estimated as <1 wt.% and ignored.

Preparation of oriented mounts and XRD analysis

15 mg cm^{-2} clay was used to record an XRD scan. An aliquot of 1.5 mL of suspension was deposited on the circular (diameter = 2.4 cm) ceramic tiles which were 3 mm thick. The suspension was filtered through the tile using a vacuum filter apparatus. The Urkut sample prepared in this way showed a low degree of preferred orientation. Glauconitic minerals generally tend to form spherical aggregates. A preparation technique by sedimentation of 15 mg cm^{-2} of material on a glass slide led to a much higher degree of preferred orientation.

All samples were measured in Bragg-Brentano geometry on a 3003TT (Seifert) diffractometer (CoKα radiation generated at 40 kV and 40 mA) equipped with an automatic divergence slit irradiating 10 mm sample length, a 0.5 mm detector slit, a diffracted beam graphite monochromator, and a scintillation counter. The patterns were collected from 2 to 60º2θ with a step size of 0.03º2θ and 5 s per step.

The specimens were stored overnight in an ethylene glycol atmosphere at 60ºC after recording a pattern under AD conditions. The clay films were measured again (in this case only 2 s per step) after cooling to room temperature, representing EG conditions.

RESULTS AND DISCUSSION

The standard deviation, σ, was declared with two significant digits, and the refined value with the same number of decimal places as σ (Tables 3–5 and 7–9). This high precision is justified in the case of simulated data because the models for refinement are identical to those which were used for the simulations. The declaration of all decimals in the case of the observed data assumed an accuracy which is not obtainable for real measurements, because all crystallographic models are just an approximation of reality, but it helps to evaluate differences between the models. σ was not declared if a refinement limit was reached. No result was declared if the parameter was kept fixed and bold letters were used for fixed values, which differ from the simulation. The R_{wp} value was declared for each refinement. The R_{wp} also depends on the measurement conditions and can only be applied directly for comparisons of refinements using the same measurement data. The comparison of results from refinements using different measurements must be seen in relation to the R_{exp} value. R_{exp} is the smallest obtainable value of R_{wp} and can be calculated from the counting statistics of the measurement (Howard and Preston, 1989).

https://doi.org/10.1346/CCMN.2012.0600507 Published online by Cambridge University Press

Table 3. Structural parameters for the simulation and refinement results of an R0 ordered I-S.

	Simul-ation	Refinement limits	— R_{wp} = 4.87% — R0 start	result	σ	— R_{wp} = 4.86% — R1 start	result	σ	— R_{wp} = 33.63% — R2 start	result	σ	— R_{wp} = 36.08% — R3 start	result	σ	— R_{wp} = 4.86% — R1, extreme start	result	σ
Repeating distances																	
t smectitic (1w) (Å)	12.5	11.65–12.85	12.5	12.5032	0.0044	12.5	12.5072	0.0046	12.5	n.r.		12.5	12.29	0.30	11.65	12.5069	0.0046
t smectitic (2w) (Å)	15	14.3–15.51	15	14.9909	0.0035	15	14.9915	0.0035	15	15.111	0.018	15	15.041	0.027	14.3	14.9916	0.0035
Atomic occupancies																	
p(Fe)	0.1	0–0.7	0.1	0.1564	0.0059	0.1	0.1615	0.0062	0.1	0.295	0.032	0.1	0.086	0.048	0.1	0.1611	0.0062
p(K)	0.8	0.6–1	0.8	0.704	0.036	0.8	0.699	0.037	0.8	0.6		0.8	0.6		0.8	0.700	0.037
p(Ca)	0.2	0.1–0.3	0.2	0.258	0.021	0.2	0.262	0.020	0.2	0.1		0.2	0.1		0.2	0.263	0.020
p(H_2O) (1w)	0.8	0–1	0.8	0.538	0.066	0.8	0.515	0.066	0.8	n.r.		0.8	1		0.8	0.514	0.066
p(H_2O) (2w)	0.6	0–1	0.6	0.731	0.037	0.6	0.737	0.037	0.6	1		0.6	1		0.6	0.735	0.037
Distance to midplane																	
d(H_2O) (Å)	1.2	1–1.5	1.2	1.220	0.032	1.2	1.235	0.031	1.2	1.5		1.2	1.5		1.2	1.234	0.031
Proportions and probabilities																	
*w*I	0.25	0*–1	0.5	0.2509	0.0040	0.5	0.2474	0.0042	0.75	0.6099	0.0019	0.875	0.667	0.013	0.99	0.2472	0.0042
*p*1w	0.5	0–1	0.5	0.5005	0.0048	0.5	0.4938	0.0054	0.5	0		0.5	0.081	0.040	1	0.4943	0.0054
*p*II (R1)		mpdo–1				0	0.2271	0.0089		0.3604 (mpdo)			0.501 (mpdo)		0.99	0.2272	0.0089
*p*III (R2)		mpdo–1							0.5	0			0 (mpdo)				
*p*IIII (R3)		mpdo–1										0.8	1				

	Simul-ation	Refimement limits	— R_{wp} = 5.32% — R1, t_S (1w) = 12.625 start	result	σ	— R_{wp} = 4.99% — R1, known occupancies start	result	σ	— R_{wp} = 4.92% — R1, incorrect *p*(Fe) start	result	σ	— R_{wp} = 5.04% — R1, incorrect *p*(Ca) start	result	σ	— *R*wp = 4.99% — R1, incorrect *p*(Ca) start	result	σ
Repeating distances																	
t smectitic (1w) (Å)	12.5	11.65–12.85	**12.625**			12.5	12.5010	0.0035	12.5	12.5130	0.0047	12.5	12.5079	0.0037	12.5	12.5003	0.0041
t smectitic (2w) (Å)	15	14.3–15.51	15	14.9781	0.0036	15	14.9906	0.0038	15	14.9908	0.0035	15	14.9885	0.0038	15	14.9911	0.0038
Atomic occupancies																	
p(Fe)	0.1	0–0.7	0.1	0.1958	0.0063	0.1			**0.2**			0.1			0.1		
p(K)	0.8	0.6–1	0.8	0.6		0.8			0.8			0.8			0.8		
p(Ca)	0.2	0.1–0.3	0.2	0.215	0.015	0.2			0.2			**0.1**			**0.3**		
p(H_2O) (1w)	0.8	0–1	0.8	0.168	0.050	0.8	0.828	0.032	0.8	0.577	0.050	0.8	0.973	0.033	0.8	0.597	0.042
p(H_2O) (2w)	0.6	0–1	0.6	1		0.6	0.703	0.031	0.6	0.836	0.034	0.6	0.820	0.031	0.6	0.635	0.035
Distance to midplane																	
d(H_2O) (Å)	1.2	1–1.5	1.2	1.376	0.017	1.2	1		1.2	1.142	0.021	1.2	1		1.2	1.100	0.030
Proportions and probabilities																	
*w*I	0.25	0*–1	0.5	0.2597	0.0037	0.5	0.2236	0.0029	0.5	0.2523	0.0034	0.5	0.2308	0.0029	0.5	0.2223	0.0034
*p*1w	0.5	0–1	0.5	0.4263	0.0045	0.5	0.5345	0.0024	0.5	0.4881	0.0035	0.5	0.5302	0.0025	0.5	0.5337	0.0031
*p*II (R1)		mpdo–1	0	0.1561	0.0093	0	0.2267	0.0094	0	0.2250	0.0088	0	0.2375	0.0091	0	0.2243	0.0096

Values in bold: Incorrect parameters. n.r.: Not refineable because the proportion of the corresponding component was zero. R_{exp} = 4.16%. *: The lower refinement limit for R2 and R3 was increased due to the definition range.

Table 4. Structural parameters for the simulation and refinement results of an R1 ordered I-S.

			— R_{wp} = 13.05% — R0			— R_{wp} = 5.17% — R1			— R_{wp} = 33.92% — R2			— R_{wp} = 32.78% — R3			— R_{wp} = 5.17% — R1, extreme		
	Simul-ation	Refinement limits	start	result	σ	start	result	σ	start	result	σ	start	result	σ	start	result	σ
Repeating distances																	
t smectitic (1w) (Å)	12.5	11.65−12.85	12.5	12.85		12.5	12.519	0.016	12.5	12.85		12.5	12.247	0.096	11.65	12.519	0.016
t smectitic (2w) (Å)	15	14.3−15.51	15	15.0226	0.0062	15	14.9904	0.0029	15	15.092	0.031	15	15.057	0.037	1.43	14.9905	0.0029
Atomic occupancies																	
p(Fe)	0.1	0−0.7	0.1	0.238	0.014	0.1	0.1377	0.0046	0.1	0		0.1	0		0.1	0.1376	0.0046
p(K)	0.8	0.6−1	0.8	0.6		0.8	0.758	0.012	0.8	0.761	0.057	0.8	1		0.8	0.757	0.012
p(Ca)	0.2	0.1−0.3	0.2	0.3		0.2	0.224	0.018	0.2	0.1		0.2	0.3		0.2	0.224	0.018
p(H_2O) (1w)	0.8	0−1	0.8	1		0.8	0.47	0.15	0.8	1		0.8	0		0.8	0.46	0.15
p(H_2O) (2w)	0.6	0−1	0.6	1		0.6	0.695	0.032	0.6	0		0.6	0.41	0.32	0.6	0.694	0.032
Distance to midplane																	
d(H_2O) (Å)	1.2	1−1.5	1.2	1.044	0.024	1.2	1.152	0.026	1.2	n.r.		1.2			1.2	1.153	0.026
Proportions and probabilities																	
*w*I	0.5	0*−1	0.5	0.2451	0.0052	0.5	0.4950	0.0020	0.75	0.8010	0.0062	0.875	0.7828	0.0088	0.01	0.4950	0.0020
*p*1w	0.2	0−1	0.5	0.1388	0.0073	0.5	0.2046	0.0027	0.5	0	0	0.5	0.279	0.035	1	0.2045	0.0027
*p*II (R1)	0.75	mpdo−1				0.0	0.7444	0.0028		0.7515 (mpdo)			0.723 (mpdo)		0	0.7445	0.0028
*p*III (R2)		mpdo−1							0.5	0.670	0.017		0.616 (mpdo)				
*p*IIII (R3)		mpdo−1										0.8	0.961	0.024			

			— R_{wp} = 5.28% — R1, known occupancies			— R_{wp} = 5.34% — R1, incorrect *p*(Fe)			——— R_{wp} = 5.29% ——— R0, illitic 51.83±0.58 wt.%			R0, smectitic 48.17±0.58 wt.%			——— R_{wp} = 5.09% ——— R1, illitic 34.6±4.8 wt.%			R1, smectitic 65.4±4.8 wt.%		
	Simul-ation	Refimement limits	start	result	σ	start	result	σ	start	result	σ	start	result	σ	start	result	σ	start	result	σ
Repeating distances																				
t smectitic (1w) (Å)	12.5	11.65−12.85	12.5	12.567	0.014	12.5	12.498	0.015	12.5	12.357	0.087	12.5	12.59	0.032	12.5	12.35	0.033	12.5	12.613	0.039
t smectitic (2w) (Å)	15	14.3−15.51	15	14.9872	0.0029	15	14.9905	0.0028	15	15.001	0.014	15	15.012	0.0032	15	14.968	0.011	15	14.994	0.0037
Atomic occupancies																				
p(Fe)	0.1	0−0.7	0.1			**0.2**			0.1	0.101	0.014	0.1	0.221	0.016	0.1	0.059	0.040	0.1	0.182	0.024
p(K)	0.8	0.6−1	0.8			0.8			0.8	0.704	0.017	0.8	0.6		0.8	0.6		0.8	0.991	0.035
p(Ca)	0.2	0.1−0.3	0.2			0.2			0.2	0.3		0.2	0.154	0.020	0.2	0.3		0.2	0.211	0.029
p(H_2O) (1w)	0.8	0−1	0.8	0.27	0.12	0.8	0.67	0.14	0.8	1		0.8	0		0.8	1		0.8	0.55	0.25
p(H_2O) (2w)	0.6	0−1	0.6	0.765	0.027	0.6	0.778	0.027	0.6	0.41	0.16	0.6	0.664	0.033	0.6	1		0.6	0.542	0.057
Distance to midplane																				
d(H_2O) (Å)	1.2	1−1.5	1.2	1.158	0.017	1.2	1.028	0.017	1.2	1.5		1.2	1.303	0.035	1.2	1		1.2	1.259	0.052
Proportions and probabilities																				
*w*I	0.5	0*−1	0.5	0.4969	0.0019	0.5	0.4952	0.0019	0.95	0.8368	0.0030	0.05	0.1546	0.0030	0.95	0.542	0.021	0.05	0.459	0.014
*p*1w	0.2	0−1	0.5	0.213	0.0025	0.5	0.1957	0.0027	0.5	0.134	0.019	0.5	0.1316	0.0035	0.5	0.258	0.018	0.5	0.2024	0.0087
*p*II (R1)	0.75	mpdo−1	0	0.7582	0.0028	0	0.7300	0.0024							0	0.682	0.018	0	0.815	0.011

Values in bold: incorrect parameters. n.r.: Not refineable because the proportion of the corresponding component was zero. R_{exp} = 4.34%. *: The lower refinement limit for R2 and R3 was increased due to the definition range.

Table 5. Structural parameters for the simulation and refinement results of an R3 ordered I-S measured under three different conditions.

			low RH, p1w = 0.9, R_{exp} = 1.61%											
			R_{wp} = 6.39%			R_{wp} = 5.36%			R_{wp} = 4.21%			R_{wp} = 3.95%		
	Simul-ation	Refinement limits	start	R0 result	σ	start	R1 result	σ	start	R2 result	σ	start	R3 result	σ
Repeating distances														
t smectitic (1w) (Å)	12.5	11.65–12.85	12.5	12.4974	0.0037	12.5	12.4995	0.0029	12.5	12.5005	0.0024	12.5	12.4992	0.0022
t smectitic (2w) (Å)	15	14.3–15.51	15	14.3		15	15.51		15	14.866	0.033	15	14.893	0.021
Atomic occupancies														
p(Fe)	0.1	0–0.7	0.1	0.1029	0.0019	0.1	0.0993	0.0016	0.1	0.1038	0.0013	0.1	0.1066	0.0012
p(K)	0.8	0.6–1	0.8	0.7838	0.0033	0.8	0.7877	0.0028	0.8	0.7976	0.0022	0.8	0.8005	0.0021
p(Ca)	0.2	0.1–0.3	0.2	0.3		0.2	0.3		0.2	0.3		0.2	0.3	
p(H_2O) (1w)	0.8	0–1	0.8	1		0.8	1		0.8	0.938	0.036	0.8	0.855	0.034
p(H_2O) (2w)	0.6	0–1	0.6	0		0.6	0		0.6	1		0.6	1	
Distance to midplane														
d(H_2O) (Å)	1.2	1.0–1.5	1.2	n.r		1.2	n.r.		1.2	1		1.2	1	
Proportions and probabilities														
wI	0.9	0*–1	0.5	0.89751	0.00058	0.5	0.90116	0.00043	0.75	0.9007	0.00034	0.875	0.90089	0.00032
p1w	0.9	0–1	0.5	1		0.5	1		0.5	0.9314	0.0049	0.5	0.9054	0.0044
pII (R1)	mpdo	mpdo–1				0.667	0.89032	0.00053		0.88975 (mpdo)			0.88999 (mpdo)	
pIII (R2)	mpdo	mpdo–1							0.5	0.87621	0.00053		0.87639 (mpdo)	
pIIII (R3)	0.866	mpdo–1										0.8	0.86749	0.00067

			high RH, p1w = 0.1, R_{exp} = 1.46%											
			R_{wp} = 7.22%			R_{wp} = 6.15%			R_{wp} = 3.93%			R_{wp} = 3.59%		
	Simul ation	Refinement limits	start	R0 result	σ	start	R1 result	σ	start	R2 result	σ	start	R3 result	σ
Repeating distances														
t smectitic (1w) (Å)	12.5	0.667–1	12.5	12.476	0.038	12.5	12.49	0.024	12.5	12.493	0.015	12.5	12.483	0.018
t smectitic (2w) (Å)	15	14.3–15.51	15	14.9843	0.0059	15	14.9839	0.0043	15	14.9884	0.0024	15	14.9916	0.0023
Atomic occupancies														
p(Fe)	0.1	0–0.7	0.1	0.1223	0.0026	0.1	0.1111	0.0021	0.1	0.1124	0.0013	0.1	0.1102	0.0012
p(K)	0.8	0.6–1	0.8	0.7994	0.0041	0.8	0.803	0.0035	0.8	0.8079	0.0022	0.8	0.8015	0.0021
p(Ca)	0.2	0.1–0.3	0.2	0.3		0.2	0.3		0.2	0.3		0.2	0.271	0.017
p(H_2O) (1w)	0.8	0–1	0.8	1		0.8	1		0.8	1		0.8	1	
p(H_2O) (2w)	0.6	0–1	0.6	1		0.6	1		0.6	1		0.6	0.829	0.025
Distance to midplane														
d(H_2O) (Å)	1.2	1.0–1.5	1.2	1		1.2	1		1.2	1.046	0.017	1.2	1.161	0.025
Proportions and probabilities														
wI	0.9	0*–1	0.5	0.88363	0.00088	0.5	0.89136	0.0006	0.75	0.89488	0.00037	0.875	0.89848	0.00044
p1w	0.1	0–1	0.5	0.1312	0.0079	0.5	0.1485	0.0059	0.5	0.1312	0.0041	0.5	0.1043	0.0044
pII (R1)	mpdo	mpdo–1				0.667	0.87811	0.00075		0.88254 (mpdo)			0.88701 (mpdo)	
pIII (R2)	mpdo	mpdo–1							0.5	0.86703	0.00058		0.87262 (mpdo)	
pIIII (R3)	0.866	mpdo–1										0.8	0.86532	0.00068

			EG intercalated, R_{exp} = 1.30%											
			R_{wp} = 5.42%			R_{wp} = 4.99%			R_{wp} = 4.26%			R_{wp} = 4.16%		
	Simul-ation	Refinement limits	start	R0 result	σ	start	R1 result	σ	start	R2 result	σ	start	R3 result	σ
Repeating distances														
tc Smectitic (EG) (Å)	16.8	16.75–16.9	16.8	16.7758	0.0045	16.8	16.7898	0.0041	16.8	16.8014	0.0033	16.8	16.8045	0.0032
Atomic occupancies														
p(Fe)	0.1	0–0.7	0.1	0.1084	0.0025	0.1	0.0902	0.0021	0.1	0.0974	0.0019	0.1	0.0999	0.0019
p(K)	0.8	0.6–1	0.8	0.7924	0.0040	0.8	0.805	0.0036	0.8	0.8036	0.003	0.8	0.8015	0.0029
p(H_2O)	0.1	0–1	0.1	0.737	0.062	0.1	1		0.1	0.653	0.057	0.1	0.480	0.057
p(EG)	1	0.1–1	1.0	1		1.0	1		1.0	1		1.0	1	
Distance to midplane														
d(CA,H_2O) (Å)	2.525	0–2.75	2.525	0.927	0.026	2.525	2.378	0.019	2.525	2.465	0.023	2.525	2.507	0.028
d(EG) (Å)	2.15	0.434–2.75	2.15	2.437	0.02	2.15	1.9234	0.0094	2.15	2.02	0.014	2.15	2.071	0.014
Proportions and probabilities														
*w*I	0.9	0*–1	0.5	0.87594	0.00094	0.5	0.89042	0.00063	0.75	0.89672	0.00046	0.875	0.89851	0.00046
*p*II (R1)	mpdo	mpdo–1				0.667	0.87693	0.00079		0.88483 (mpdo)			0.88704 (mpdo)	
*p*III (R2)	mpdo	mpdo–1							0.5	0.86996	0.00072		0.87266 (mpdo)	
*p*IIII (R3)	0.866	mpdo–1										0.8	0.86583	0.00081

Values in bold: incorrect parameters. n.r.: Not refineable because the proportion of the corresponding component was zero. *: The lower refinement limit for R2 and R3 was increased due to the definition range.

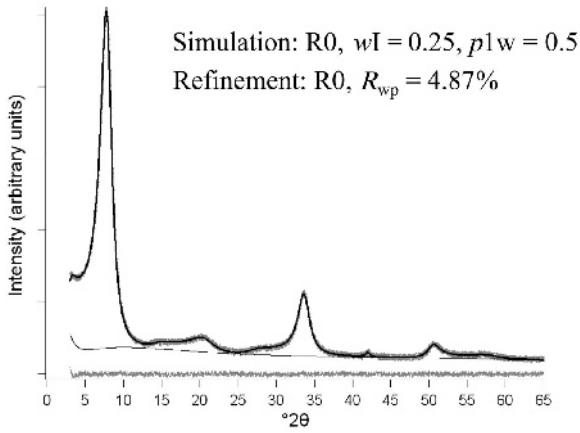

Figure 3. Simulated pattern of an R0 ordered I-S. Refinement with an R0 model.

Rietveld refinement of simulated patterns: AD I-S, R0 disordered, high smectite content

The first example was a calculated pattern of an AD I-S with a content of wS = 0.75 smectitic layers and a proportion of monohydrated smectitic layers of p1w = 0.5. The stacking was R0 disordered. Only two statistical parameters had to be considered, wI = 1 − wS and p1w.

In a first step, all four models for AD I-S were applied (Table 3). The refinements using the models for R2 and R3 obviously failed, as indicated by R_{wp} = 33.63% (R2) and R_{wp} = 36.08% (R3). In contrast, the refinements with the R0 and the R1 model had nearly identical, low R_{wp} values of 4.87% and 4.86%. The inspection of the patterns also showed two almost identical refinement results (Figures 3, 4). A plot of pII *vs*. wI (Figure 5), as proposed by Bethke *et al.* (1986), represents all possible combinations of the R1 statistical parameters. This plot shows that the R1 model can also describe the case of R0 ordering. All points on the diagonal line represent random R1 ordering or R0 ordering (pII = wI). The point 'S' represents the

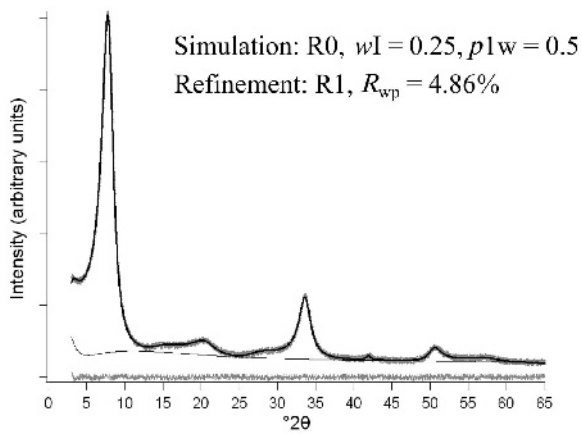

Figure 4. Simulated pattern of an R0 ordered I-S. Refinement with an R1 model.

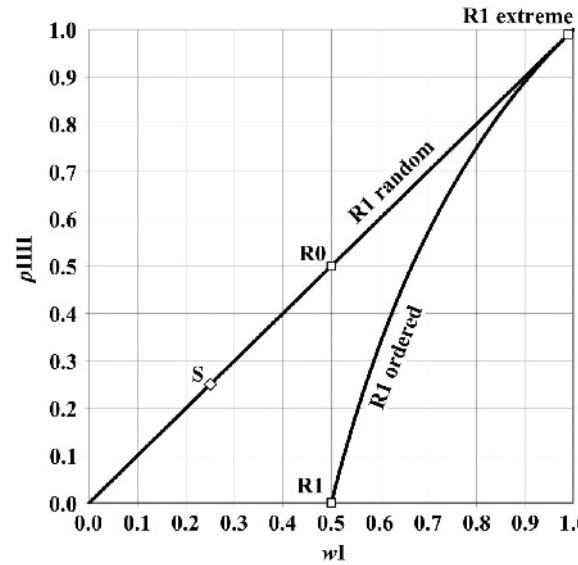

Figure 5. Junction probability diagram for R1 ordering, modified from Bethke *et al.* (1986). S: values for simulation; R0: starting values for the R0 model; R1: starting values for the R1 model; R1 extreme: extreme starting values for the R1 model.

simulation parameters; 'R0,' the starting parameters for the R0 model; and 'R1,' the starting parameters for the R1 model. These R1 starting parameters describe an ordered stacking of I-S sequences, which corresponds to the mineral rectorite. Both models fitted the translations and statistical parameters quite well, which influence the position of intensity maxima. Only the value of pII for model R1 was slightly too low. This additional refineable parameter, which is not necessary to fit the simulated data, showed a small deviation from the correct value. In contrast, it led to a slightly better R_{wp} value. At this point, it was difficult to decide which model was the correct one.

Refinements have the general problem that the minimum of differences between observed and calculated data obtained may be a local minimum in the parameter space. Other (better) solutions may be possible. One way to test for alternative solutions is to repeat the refinement with different starting parameters. Some parameters of the R1 model were set to extreme starting values for this purpose (point 'R1 extreme' in Figure 5). The starting value of the two smectitic translations was set to t_s(1w) = 11.65 Å and t_s(2w) = 14.3 Å, the smallest values in the considered refinement range. The statistical parameters wI and pII were set to 0.99 (Figure 5) and p1w = 1. The results of this refinement were nearly identical to those of the previous refinements with R0 and R1 model, although the starting parameters described a practically pure illite. This gave a strong indication that the R_{wp} value of 4.86% obtained with the R1 model was the best possible result with this set of parameters.

https://doi.org/10.1346/CCMN.2012.0600507 Published online by Cambridge University Press

The refinement of the occupancies of the cations and the interlayer water failed in all of these first five refinements, indicating that the intensity-affecting parameters were difficult to refine while the position-affecting parameters could be obtained with high accuracy. In a further refinement, the parameter t_s(1w) was fixed to a slightly incorrect value to test the sensitivity of the refinement of the position-affecting parameters. The value t_s(1w) = 12.625 Å is 1% too high, and the refinement led to a reduced R_{wp} of 5.32%. The refinement pattern showed an abnormal run of the background line and the positions of the intensity maxima deviated slightly, as indicated by the difference line (Figure 6). No other refined parameter could compensate for the incorrect t_s(1w).

Supporting analysis results for the chemical composition were introduced in the next refinements. The occupancies of Fe, K, and Ca were kept fixed to the correct values. These values can be derived from XRF analysis, for example. The occupancy of the water molecules and the distance to the midplane in the 2w state were still refined. These values depend upon the environmental conditions and are difficult to control and determine. The translations and probabilities were set to the correct values and refined. The R_{wp} value of 4.99% increased slightly with respect to the previous refinements. The pattern (not shown) can scarcely be distinguished from Figures 3 or 4.

Occupancies calculated from XRF data may be biased by unidentified additional components. The value for Fe was doubled in a further refinement. Iron can be overestimated, for example, if poorly crystalline Fe (oxyhydr)oxides are missed in the qualitative examination. Refinement with an incorrect Fe occupancy led to a slightly better R_{wp} (4.92%) than the refinement with the correct occupancies. An inspection of the pattern showed that the background line of this refinement had an abnormal run below 10º (Figure 7). The intensity of the first maximum was calculated at too high a level due to

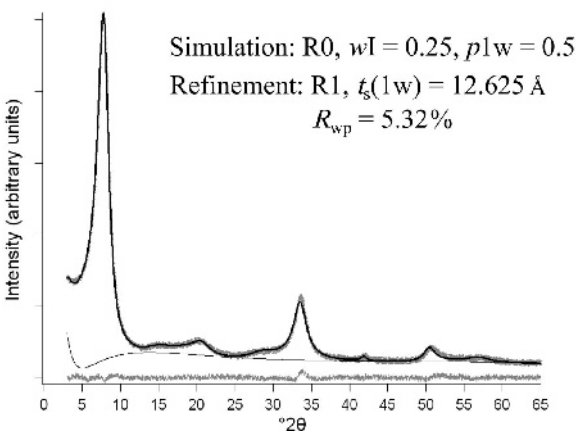

Figure 6. Simulated pattern of an R0 ordered I-S. Refinement with an R1 model and t_s(1w) = 12.625 Å.

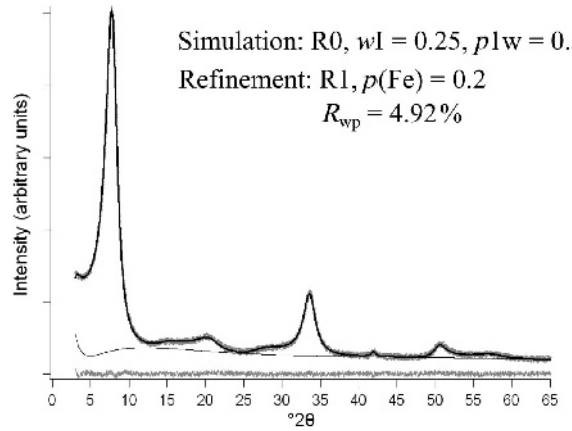

Figure 7. Simulated pattern of an R0 ordered I-S. Refinement with an R1 model and p(Fe) = 0.2.

the incorrect Fe content. This was compensated by a decay of the background line.

The Ca occupation was set to incorrect values in two additional refinements, one 0.1 too low and one 0.1 too high. The resulting R_{wp} values (5.04% for p(Ca) = 0.1 and 4.99% for p(Ca) = 0.3) were again close to the optimum value of 4.86%. The patterns were similar to that of the optimum refinement and no unusual detail could be noticed.

This example showed that identifying the nature of the disordering is possible by applying the four different models only. The incorrect models R2 and R3 could easily be identified by their very high R_{wp} values. The results of the R0 and R1 models were identical, allowing for standard deviation. The translations and probabilities could be reproduced with high precision, even with inappropriate starting parameters. The refinement of occupancies and the position of the water molecules in the 2w interlayer failed in all cases. Even with the preset of the initial cation occupancies, obtaining correct water parameters was not possible. Incorrect occupancies of Fe and Ca were compensated by other parameters. Five refinements with different results led to similar R_{wp} values in the restricted range of 4.86–5.04%. Inspection of the patterns indicated erroneous results in one case (p(Fe) = 0.2). The other four patterns gave no indication of incorrect parameters.

Rietveld refinement of simulated patterns: AD I-S, R1 ordered, intermediate smectite content

The second example is a calculated pattern of an AD I-S with equal amounts of illitic and smectitic layers (wI = wS = 0.5). The proportion of monohydrated smectitic layers is now smaller than that of bihydrated layers (p1w = 0.2). The stacking is R1 ordered with the stacking probability pII = 0.75. Points which plot in the area above the random ordering diagonal of the junction probability diagram (Figure 5) show tendencies of segregation. In the extreme case of pII = 1 a physical

https://doi.org/10.1346/CCMN.2012.0600507 Published online by Cambridge University Press

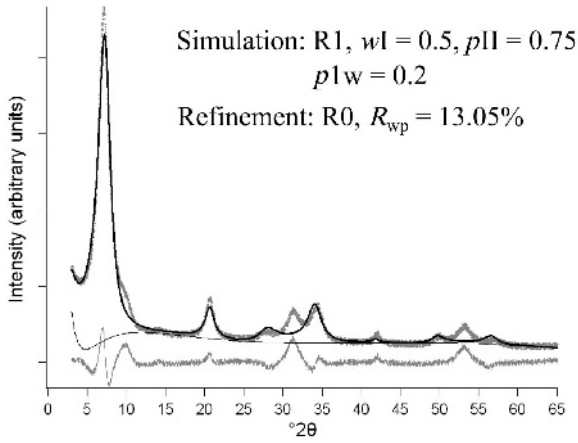

Figure 8. Simulated pattern of an R1 ordered I-S. Refinement with a R0 model.

mixture is present. The value of pII in this example was half way between random stacking and a physical mixture.

All four models for AD I-S were again applied as a first step (Table 4). R2 and R3 showed very high R_{wp} values of 33.92% (R2) and 32.78% (R3). They could be ruled out. The R_{wp} value of the refinement with the R0 model was clearly lower (13.05%) but the pattern still showed remaining intensities (Figure 8). The refinement with the R1 model led to the best result (R_{wp} = 5.17%, Figure 9). The parameters affecting the position of the intensity maxima were again well reproduced. An additional refinement with extreme starting values (wI = 0.01, p1w = 1 and pII = 0) confirmed that this was the optimum fit. The refined occupancies were satisfying, considering a deviation of three times σ. Just the occupancy of the water molecules in the monohydrated interlayers showed a strong discrepancy from the correct value and a high standard deviation. Only 10% of all layers (p1w · wS · 100%) were monohydrated smectitic layers, and therefore the influence of this component on the diffraction pattern was small and refinements of the corresponding parameters showed strong uncertainties.

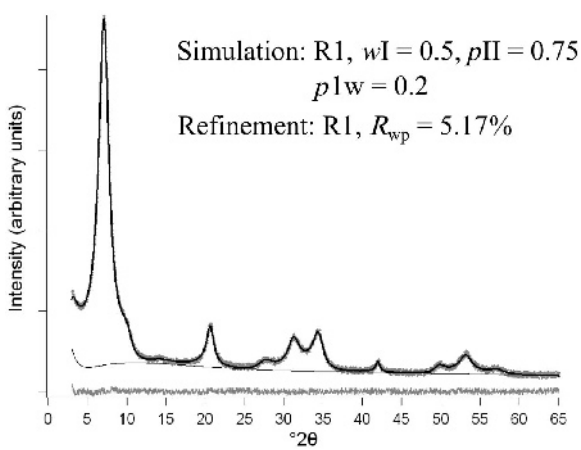

Figure 9. Simulated pattern of an R1 ordered I-S. Refinement with an R1 model.

Additional information about the cation occupancies was added in the next refinements; one refinement with the correct values for p(Fe), p(K), and p(Ca) and another refinement with an incorrect Fe content (p(Fe) = 0.2). The R_{wp} values increased slightly (5.28% and 5.34%, respectively), the occupancy of water in the monohydrated interlayer again showed a strong uncertainty, but the translations and statistical parameters were again in good agreement with the correct values. The pattern of the refinement with the correct values showed no suspicious details and was similar to the optimum fit. The pattern of the refinement with the incorrect Fe content showed the same abnormal run as in the first example, indicating errors in the model.

The refinement with the R0 model led to better results than the refinements with the R2 and R3 models as already mentioned but the result was still not satisfactory. A different interpretation of this refinement might be that it was a mixture of more than one I-S mineral. The remaining intensity in the difference line (Figure 8) showed peaks at 10.4 Å, 5.0 Å, 3.3 Å, and 2.0 Å. These positions could be assigned to an I-S with high proportion of illitic layers, while the refined model resulted in an I-S with low illitic proportion (wI = 0.2451). A refinement with two R0 models was performed, therefore; one starting with a high proportion of illitic layers (wI = 0.95) and one with a low proportion (wI = 0.05). The R_{wp} of this refinement (5.29%) was on the order of the refinements with the correct R1 model. The refined parameters reflected a mixture of an illitic- and a smectitic-dominated I-S of nearly equal contents (51.83 wt.% and 48.17 wt.%) but the pattern showed a physically unsound run of the background line at low angles (Figure 10). Several occupations reached the refinement limits. The use of two different R0 models gave unsatisfactory results.

A refinement with two different R1 models (wI = 0.95 and 0.05) decreased the R_{wp} to 5.09%, the best value of all refinements for this example. The pattern showed no unusual details (Figure 11), but again several parameters reached the refinement limits or had incorrect values. The proportions of illitic layers wI and stacking probability pII converged toward the correct value. The mean value of these two pairs of parameters was almost identical to the correct value. The two I-S had different contents (34.6 wt.% and 65.4 wt.%), but the shape and position of the intensity maxima were nearly identical. This observation indicated that the choice of just one model was closer to the initial simulation model, although the R_{wp} value of a refinement with just one R1 model was slightly greater. The tendency of segregation of the input structure was also reflected.

https://doi.org/10.1346/CCMN.2012.0600507 Published online by Cambridge University Press

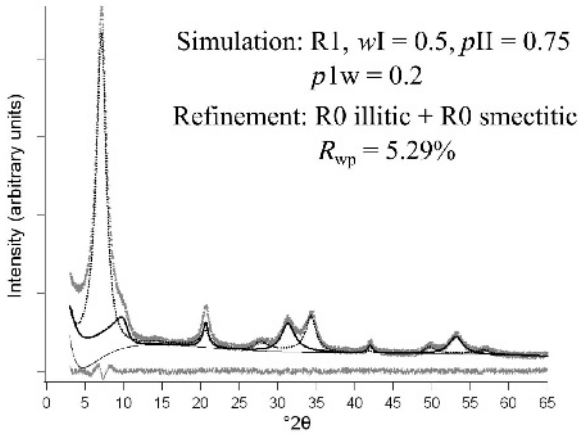

Figure 10. Simulated pattern of an R1 ordered I-S. Refinement with two R0 models. Black line: illite-dominated I-S; dotted line: smectite-dominated I-S. The overall sum of all calculated lines was not shown.

This example also showed that the application of all four models facilitated the identification of the stacking order. That the models R2 and R3 were incorrect could be established because the difference in the R_{wp} value was large enough. The correct R1 model clearly led to the best R_{wp} value of all four models. Inspection of the R0 refinement pattern offered a second interpretation, suggesting that the simulated data be viewed as a measurement of a mixture. Both tests, using just one R1 model or a mixture of two R1 models with different starting values, led to results of good statistical quality. Only a deeper interpretation showed that the use of just one model produced results closer to the correct values.

The refinement of occupancies in this example was more successful than in the first example. The structure contained fewer smectitic interlayers. The number and position of the water molecules were the main source of uncertainty.

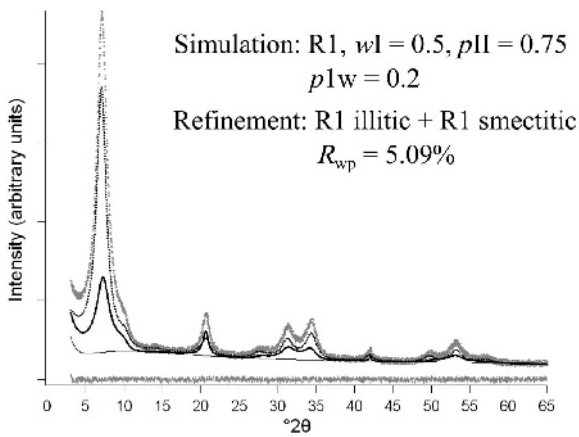

Figure 11. Simulated pattern of an R1 ordered I-S. Refinement with two R1 models. Black line: illite-dominated I-S; dotted line: smectite-dominated I-S. The overall sum of all calculated lines was not shown.

Rietveld refinement of simulated patterns: I-S, R3 ordered, low smectite content

The third example showed how to apply the Rietveld models in a multi-specimen analysis (Sakharov *et al.*, 1999). The material considered was an R3 ordered I-S with a large proportion of illitic layers (wI = 0.9). The R1 and R2 stacking probabilities showed the maximum possible degree of ordering, so the stacking probabilities were pII = (2 · wI − 1)/wI = 0.8889 and pIII = (3 · wI − 2)/(2 · wI − 1) = 0.875. The stacking parameter pIIII was set to 0.866, describing a partially ordered stacking between R3 random ordering and R3 (mpdo) ordering. The junction probability diagram (Figure 12) shows that the gap between random ordering and mpdo became smaller for increasing wI. The difference between pIIII (mpdo) = 0.8571 and pIII (mpdo) for wI = 0.9 was only 0.0179 and the chosen value of pIIII was close to both cases. The R2 model cannot reflect this kind of ordering, but R2 (mpdo) is very similar to it. An accurate examination of the patterns to determine the stacking nature was necessary. Two different patterns for AD material were calculated with two different values of p1w to simulate measurements under low (p1w = 0.9) and high (p1w = 0.1) relative humidity. An additional calculation was performed assuming that the material was ethylene glycol intercalated. The synthetic noise of the measurements was reduced in contrast to the former calculations to simulate better counting statistics.

The variation of the hydration states and intercalation species did not change the stacking sequence and inner structure of the TOT layers, but all three patterns (Figure 13) showed different intensity maximum posi-

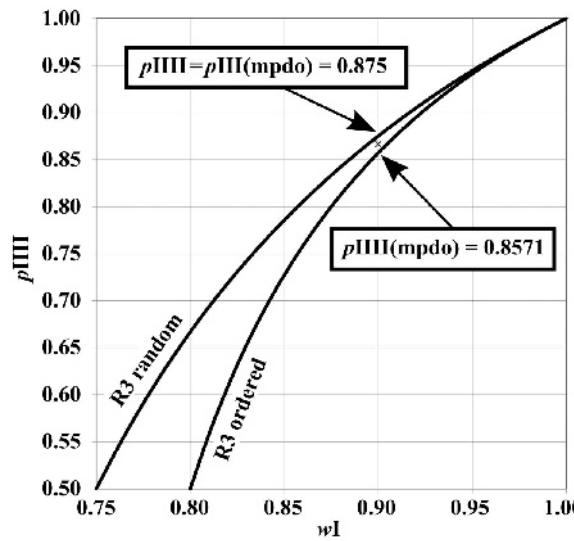

Figure 12. Junction probability diagram for R3 ordering, modified from Bethke *et al.* (1986). The pIIII value used for the simulation lies in the space between R3 ordered and R3 random.

https://doi.org/10.1346/CCMN.2012.0600507 Published online by Cambridge University Press

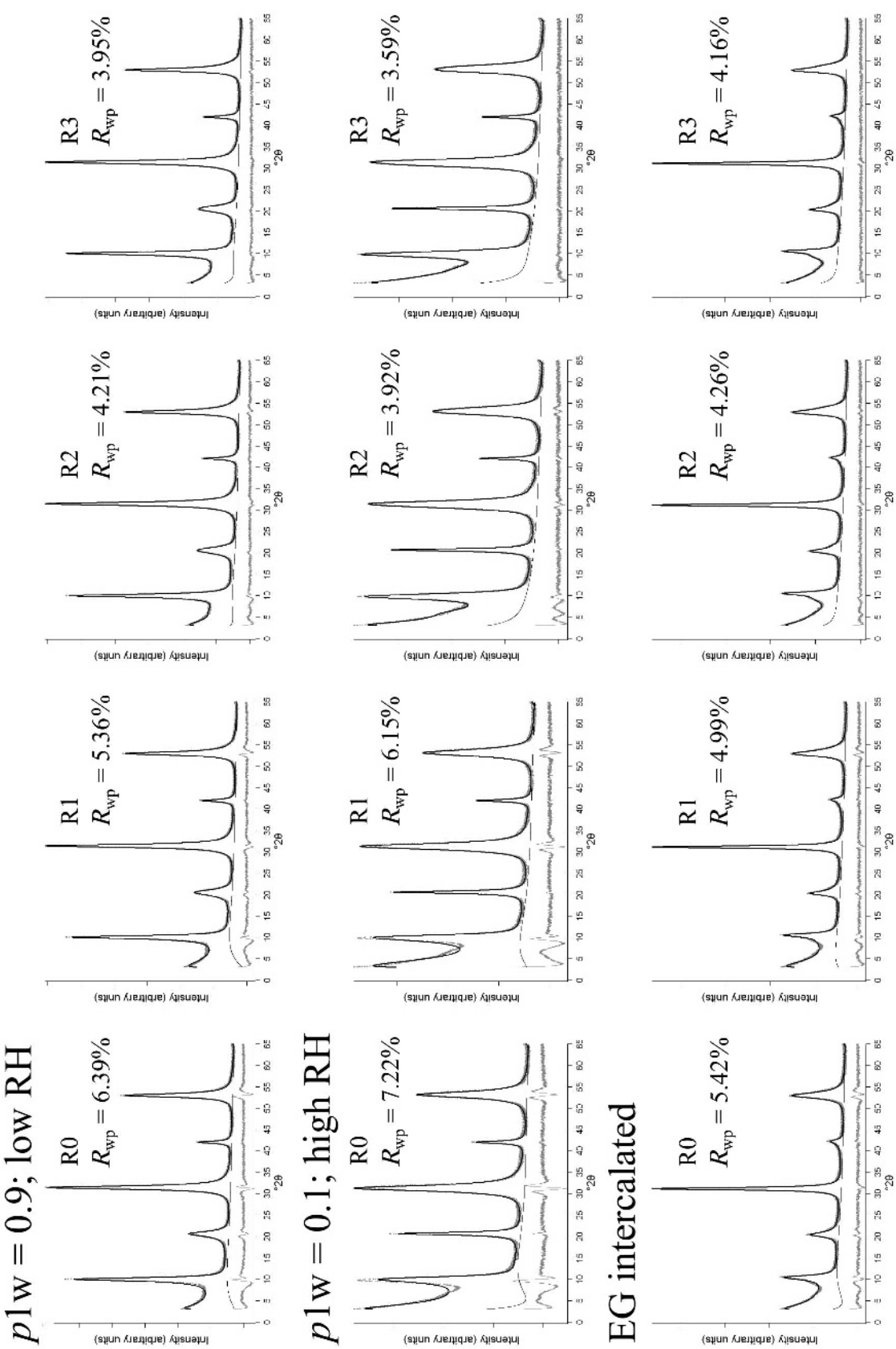

Figure 13. Simulated patterns of an R3 ordered I-S calculated for different conditions and refinements with all four models. First row: simulation of AD material measured under low relative humidity. Second row: simulation of AD material measured under high relative humidity. Third row: simulation of EG-intercalated material.

https://doi.org/10.1346/CCMN.2012.0600507 Published online by Cambridge University Press

tions due to a change of proportions ($p1w$) and repeating distances (t_s). The intensity distributions also changed because the atomic content of the smectitic interlayers had changed.

Each pattern was refined four times with the different Reichweite models (Table 5, Figure 13). The R_{wp} values obtained decreased with increasing degree of R. The correct R3 model systematically led to the best results, but even the worst R_{wp} values were not as high as in the other examples. All models fitted, at least roughly, the positions and intensity ratios of all maxima.

The refinements with the R0 and R1 models showed an unusual run of the background line and discrepancies were clearly visible in the difference line. The use of the R2 models increased the quality of the refinement, as indicated by the lower R_{wp} values. The refinements with the R3 models showed the lowest R_{wp} values, but the differences between the R2 and R3 values were relatively small. In the case of EG intercalation it was only 0.1%. A clear hint that the R2 model was not correct is that the modulation of the simulated pattern at angles below 10º could not be reproduced by this model, especially in the case of high RH.

No chemical information on the occupancies was used in these refinements but all models provided good results for the occupancies of Fe and K. The refinement of the occupancies and positional parameters of the smectitic interlayers failed even for the correct R3 model. The proportion of these components only had a small influence on the diffraction of the whole stack and the refinement results were inaccurate. Remarkably, even the R0 and R1 models led to a correct proportion of illitic layers.

This example again showed that the application of all models helps to identify the correct nature of disorder, but the contrast of the R_{wp} values now was not as clear as for samples with lower illitic content. The R2 and R3 models, in particular, both led to reasonable results and only the careful inspection of the small-angle modulations allowed a differentiation. This requires high-quality data.

The difficulty becomes less severe for R3-ordered materials with lower illitic content, as might be expected because the lines of R3 ordered and R3 random diverge with decreasing wI (Figure 12). R2 and R3 ordered I-S with greater wI become virtually indistinguishable, however. This example highlights the importance of error evaluation for the use of the terminology in the classification of mixed-layer minerals.

Characterization of sample material

The results of the chemical analysis of the same samples were used as an independent test of the reliability of the refinements. The structural formulae calculated from the XRF data (Table 6) were corrected due to the estimated quartz content. The resulting uncertainties in the Si content may bias the Al-Mg-Fe-ratio at the octahedral positions for which attempts were made to refine. The following formulae were determined using this method:

Urkut: $Ca_{0.04}K_{0.71}Si_{3.91}Al_{0.09}(Al_{0.50}Fe_{0.83}Mg_{0.65})O_{10}(OH)_2$.
ISCz-1: $Ca_{0.09}K_{0.48}Si_{3.52}Al_{0.48}(Al_{1.70}Fe_{0.08}Mg_{0.24})O_{10}(OH)_2$.
F4: $Ca_{0.06}K_{0.67}Si_{3.41}Al_{0.59}(Al_{1.73}Fe_{0.03}Mg_{0.26})O_{10}(OH)_2$.

The composition calculated for ISCz-1 was consistent with the reference formula from the CMS website (http://www.clays.org/SOURCE%20CLAYS/SCdata.html) and Gailhanou *et al.* (2007).

Rietveld refinements from real measured patterns were performed under more realistic conditions than those from simulated values. For example, all XRD patterns showed weak peaks from impurities. The Urkut and F4 samples contain quartz and ISCz-1 contains kaolinite as minor constituents and all patterns (except those prepared on glass slides) showed corundum reflections which are produced by the ceramic tile. These reflections were introduced into the refinement by suitable structure models. The patterns of the Urkut sample showed some *hkl* reflections from glauconite. In general, glauconites tend to form spherical aggregates which hamper the orientation of the particles in the prepared samples. These reflections were ignored here.

Rietveld refinement of data: Urkut glauconite-smectite

Both patterns of the Urkut sample, measured under AD conditions and after EG solvation, were refined with models considering all four Reichweite degrees. The R_{wp} values for the AD state were close, at 11.89% and 13.46%, while those of the EG state were 12.88% and 13.21%. The best value was achieved for R1 ordering in case of AD and for R2 ordering in the case of EG intercalation. A comparison of the patterns (Figure 14) showed that the refinements using the AD material with models R1 to R3 had a modulated run of the calculated line in the range 2–9º2θ, which was not present in the observed diffraction line. This effect was less

Table 6. XRF data of the test materials (wt.% oxides).

Sample	SiO_2	TiO_2	Al_2O_3	Fe_2O_3	MnO	MgO	CaO	Na_2O	K_2O	LOI	Total
Urkut	59.1	0.2	6.3	13.8	0.2	5.5	0.5	0.0	7.0	7.2	99.8
IS-Cz1	50.7	0.1	25.7	1.5	0.0	2.2	1.1	0.0	5.2	13.1	99.7
F4	51.7	0.1	27.6	0.6	0.0	2.5	0.6	0.0	7.3	9.3	99.7

https://doi.org/10.1346/CCMN.2012.0600507 Published online by Cambridge University Press

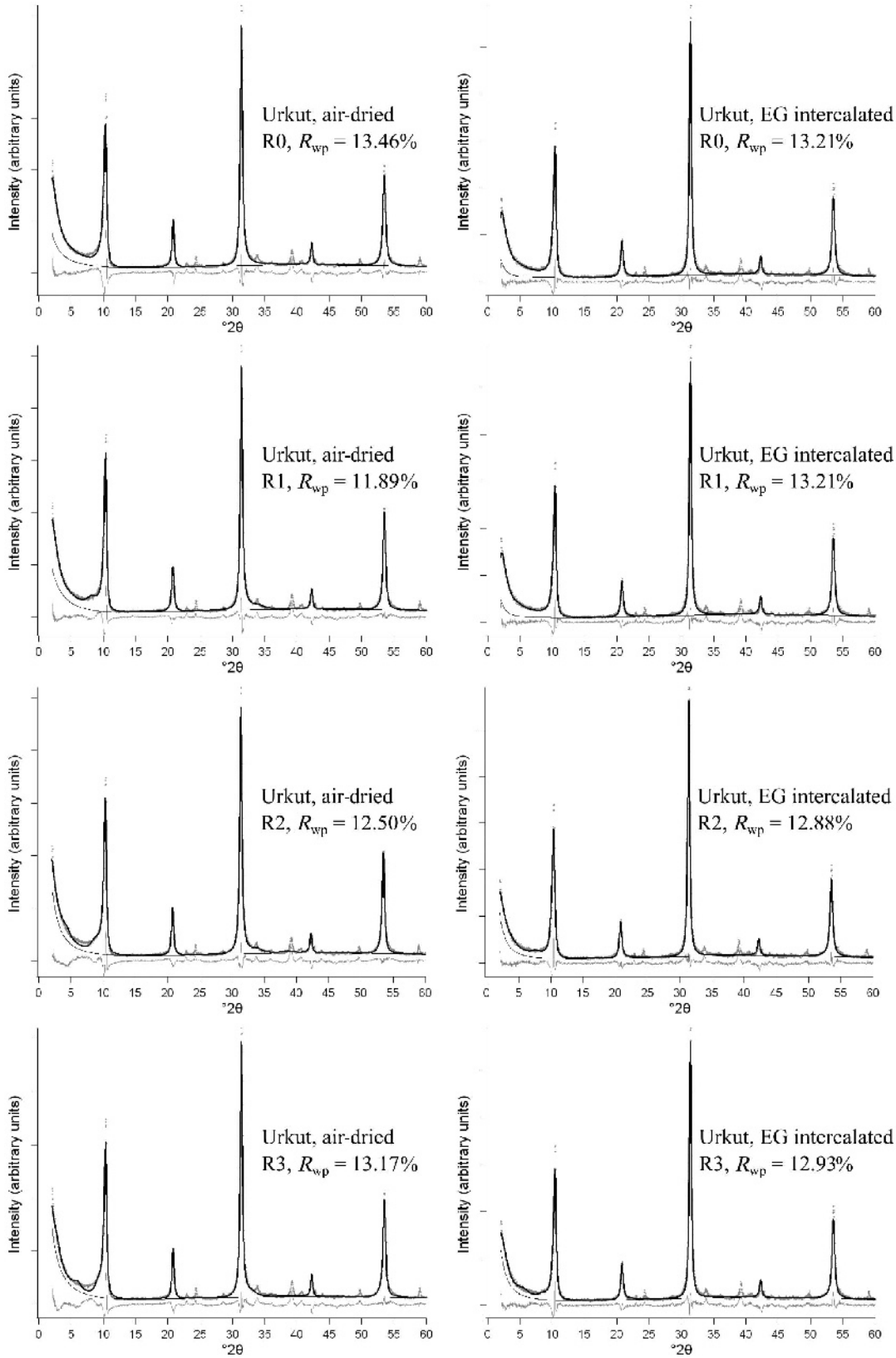

Figure 14. Refinements of sample Urkut in AD and EG state refined with all four models. The calculated line of the quartz peaks was not shown.

https://doi.org/10.1346/CCMN.2012.0600507 Published online by Cambridge University Press

pronounced in the case of EG intercalation but still observable. Only the two refinements with the R0 model both showed an unmodulated run at small angles. This suggests that the stacking order of this material could be described with R0 disorder, though the R_{wp} values were not the smallest obtained. The refined values of the probability parameters *p*II (R1), *p*III (R2), and *p*III (R3) were indeed very near to the proportion of glauconitic layers (Table 7). The observation that all models led to comparable R_{wp} values agreed with the previous finding, that the degree of Reichweite was difficult to determine for samples with large illite contents.

The small number of smectitic layers ($wS < 0.053$) was obviously the reason that the parameters related to the smectitic layers (t_s, *p*1w, and occupancies of interlayer atoms/molecules) were not satisfactorily refineable. They all reached a refinement limit or showed high standard deviations.

The refined values of the occupancies *p*(Fe) and *p*(K) were very close for all eight refinements. The mean values of the two R0 refinements were *p*(Fe) = 0.44 and *p*(K) = 0.69. Occupancies can also be calculated from the structural formula. The K content in the formula was divided by the fraction of glauconitic layers, as this value referred to the whole mineral while *p*(K) from the Rietveld refinement only referred to the glauconitic interlayers. A value of 0.97 was considered for *w*I, the mean value of the two R0 refinements. This led to an occupancy of K calculated from the chemical formula of $p(K)_{chem} = 0.71/0.97 = 0.73$. This quantity was only slightly greater than the refined value of *p*(K). The value for Fe in the structural formula had to be divided by two, because this formula contained two octahedral positions while the refined value referred to just one position. $p(Fe)_{chem} = 0.83/2 = 0.42$ was in good agreement with the refined value.

The results of these two parameters supported the conclusion from example 3 that Fe in the TOT layer and K in the illitic (glauconitic) interlayer could be refined reliably for stackings with small smectitic contents.

Rietveld refinement of data: ISCz-1 illite-smectite

The ISCz illite-smectite sample was also refined with all four models in both states (Table 8). Only the refinements with the R1 and R2 models led to acceptable results with R_{wp} values of 9.34% (R1, AD), 8.65% (R2, AD), and 12.39% (both models, EG). The R_{wp} values of the refinements with the R0 and R3 models were more than twice as large and could be ruled out. The R2 model led to a better R_{wp} value than the R1 model while the refinements of the EG-intercalated state were statistically equivalent with slightly different results. The refined parameters of the two refinements in the AD state corresponded quite well. All four patterns (Figure 15) showed differences of the measured and the calculated line but, in general, peak positions and intensity ratios were in agreement.

The average proportion of illitic layers was refined as $wI = 0.715$ for the pattern of the AD material, while the value from the EG-intercalated state was slightly lower ($wI = 0.683$).

The refined *p*II values of the two R1 refinements came very close to the mpdo condition (Figure 16). The refinement with the R2 model in the case of EG intercalation fulfilled the condition of R2 random ordering, which is identical to the case of maximum ordering in R1 ordered stacking. Only the refinement with the R2 model in the AD state led to a result which differed from the condition of R1 (mpdo) ordering. *p*III was slightly larger than *p*II, which implied a weak tendency towards segregation of illitic units.

The probability that a smectitic layer is in the monohydrated state was quite small (*p*1w = 0.125, average value). This was consistent with the general observation that the 2w state is the dominant state of smectites in a temperate climate with 30−50% RH and with Ca intercalation. The overall proportion of the 1w layer type was $wS(1w) = wS \cdot p1w = 0.036$. This small fraction made only a minor contribution to the diffraction pattern, which caused refinement of the corresponding parameters, t_s and $p(H_2O)$ of the 1w state, to be problematic as they reached a refinement limit. *p*(Ca) reached the lower limit of 0.1, although it corresponded also to the more pronounced 2w state. $p(Ca)_{chem}$ was calculated from the structural formula as $0.09/wS = 0.32$. This showed that the refinement of *p*(Ca) failed. This occupancy is correlated significantly with the water content and difficult to refine. $d(H_2O)$ and $p(H_2O)$ could be refined within their refinement limits, but no independent observation was available to check the reliability. The t_s value of the 2w state could be refined to a realistic value of 14.95 Å, even with the failing R0 model. The refinements of the simulated data showed that the refinement of translations is reliable.

The occupancies of Fe and K calculated from the structural formula were $p(Fe)_{chem} = 0.08/2 = 0.04$ and $p(K)_{chem} = 0.48/wI = 0.67$. The refinement results for *p*(Fe) = 0.044 and *p*(K) = 0.618 (average values) in the case of the AD differed from the values calculated from the structural formula, but were of the same magnitude. The refined value of *p*(K) = 0.659 from the EG-intercalated state was even closer to the value calculated from the structural formula. But the refinement of *p*(Fe) failed. The result was more than twice the value deduced from the structural formula.

These results showed that the reliability of the refinement of *p*(Fe) and *p*(K) decreases with increasing proportion of smectitic layers.

Rietveld refinement of observed data: illite-smectite F4

The patterns of sample F4 in both states were also refined using all four models (Table 9). The R_{wp} values of the refinements with the R0 and R1 models were >20%. These models were excluded as potential

https://doi.org/10.1346/CCMN.2012.0600507 Published online by Cambridge University Press

Table 7. Refinement results of the G-S Urkut sample in air-dried (AD) and EG-intercalated states. Each state was refined with four different models (R0 to R3).

		AD, R_{exp} = 3.678%											
		— R_{wp} = 13.46% —			— R_{wp} = 11.89% —			— R_{wp} = 12.50% —			— R_{wp} = 13.17% —		
	Refinement limits	R0 start	R0 result	R0 σ	R1 start	R1 result	R1 σ	R2 start	R2 result	R2 σ	R3 start	R3 result	R3 σ
Repeating distances													
t smectitic (1w) (Å)	11.65–12.85	12.5	12.85		12.5	12.300	0.032	12.5	12.345	0.056	12.5	12.704	0.063
t smectitic (2w) (Å)	14.3–15.51	15	14.450	0.029	15	14.3		15	14.3		15	14.422	0.033
Atomic occupancies													
p(Fe)	0–0.7	0.1	0.4492	0.0067	0.1	0.4347	0.0059	0.1	0.4523	0.0063	0.1	0.4469	0.0067
p(K)	0.6–1	0.8	0.6931	0.0076	0.8	0.6767	0.0067	0.8	0.6667	0.0072	0.8	0.6792	0.0076
p(Ca)	0.1–0.3	0.2	0.1		0.2	0.1		0.2	0.1		0.2	0.1	
p(H_2O) (1w)	0–3	0.8	0		0.8	2.60	0.28	0.8	3		0.8	1.75	0.75
p(H_2O) (2w)	0–3	0.6	3		0.6	2.3	1.2	0.6	3		0.6	3	
Distance to midplane													
d(H_2O) (Å)	1.0–1.5	1.2	1.5		1.2	1.5		1.2	1.5		1.2	1.5	
Proportions and probabilities													
*w*I	0*–1	0.5	0.9616	0.0013	0.5	0.9470	0.0018	0.75	0.9496	0.0013	0.875	0.9583	0.0014
*p*1w	0–1	0.5	0.348	0.022	0.5	0.846	0.023	0.5	0.301	0.026	0.5	0.312	0.028
*p*II (R1)	mpdo–1				0	0.9755	0.0012		0.9470 (mpdo)			0.9565 (mpdo)	
*p*III (R2)	mpdo–1							0.5	0.9687	0.0014		0.9545 (mpdo)	
*p*IIII (R3)	mpdo–1										0.8	0.9717	0.0015

		EG intercalated, R_{exp} = 5.73%											
		— R_{wp} = 13.21% —			— R_{wp} = 13.21% —			— R_{wp} = 12.88% —			— R_{wp} = 12.93%		
	Refinement limits	R0 start	R0 result	R0 σ	R1 start	R1 result	R1 σ	R2 start	R2 result	R2 σ	R3 start	R3 result	R3 σ
Repeating distances													
t smectitic (EG) (Å)	16.75–16.9	16.8	16.877	0.028	16.8	16.881	0.028	16.8	16.798	0.026	16.8	16.821	0.026
Atomic occupancies													
p(Fe)	0–0.7	0.1	0.4379	0.0063	0.1	0.4374	0.0063	0.1	0.4391	0.0061	0.1	0.4401	0.0061
p(K)	0.6–1	0.8	0.6905	0.0074	0.8	0.6903	0.0074	0.8	0.6876	0.0072	0.8	0.6865	0.0072
p(H_2O)	0–2	0.1	2		0.1	2		0.1	2		0.1	2	
p(EG)	0.2–2	1.0	0.52	0.17	1.0	0.53	0.17	1.0	0.88	0.11	1.0	0.75	0.11
Distance to midplane													
d(Ca,H_2O) (Å)	0–2.75	2.525	2.71	0.13	2.525	2.72	0.13	2.525	2.75		2.525	2.75	
d(EG) (Å)	0.434–2.75	2.15	2.75		2.15	2.75		2.15	2.75		2.15	2.75	
Proportions and probabilities													
*w*I	0*–1	0.5	0.97944	0.00098	0.5	0.9800	0.0013	0.75	0.9726	0.0011	0.875	0.97527	0.00097
*p*II (R1)	mpdo–1				0	0.9797	0.0010		0.9718 (mpdo)			0.9746 (mpdo)	
*p*III (R2)	mpdo–1							0.5	0.97785	0.00096		0.9740 (mpdo)	
*p*IIII (R3)	mpdo–1										0.8	0.97920	0.00096

*: The lower refinement limit for R2 and R3 was increased due to the definition range.

Table 8. Refinement results of the I-S ISCz-1 sample in air-dried (AD) and EG-intercalated states. Each state was refined with four different models (R0 to R3).

		AD, R_{exp} = 6.28%											
		— R_{wp} = 23.06% —			— R_{wp} = 9.34% —			— R_{wp} = 8.65% —			— R_{wp} = 23.24% —		
	Refinement limits	R0 start	R0 result	R0 σ	R1 start	R1 result	R1 σ	R2 start	R2 result	R2 σ	R3 start	R3 result	R3 σ
Repeating distances													
t smectitic (1w) (Å)	11.65–12.85	12.5	12.586	0.019	12.5	12.85		12.5	12.85		12.5	n.r.	
t smectitic (2w) (Å)	14.3–15.51	15	14.946	0.014	15	14.946	0.0044	15	14.954	0.0041	15	14.910	0.012
Atomic occupancies													
p(Fe)	0–0.7	0.1	0		0.1	0.0453	0.0061	0.1	0.0417	0.0056	0.1	0.012	0.013
p(K)	0.6–1	0.8	0.6		0.8	0.6176	0.0083	0.8	0.6187	0.0075	0.8	0.6	
p(Ca)	0.1–0.3	0.2	0.3		0.2	0.1		0.2	0.1		0.2	0.1	
p(H_2O) (1w)	0–3	0.8	1.32	0.17	0.8	3		0.8	3		0.8	n.r.	
p(H_2O) (2w)	0–3	0.6	3		0.6	2.000	0.020	0.6	1.966	0.019	0.6	2.544	0.066
Distance to midplane													
d(H_2O) (Å)	1.0–1.5	1.2	1.173	0.024	1.2	1.431	0.011	1.2	1.458	0.011	1.2	1.5	
Proportions and probabilities													
*w*I	0*–1	0.5	0.6417	0.0041	0.5	0.7132	0.0011	0.75	0.7171	0.0011	0.875	0.7699	0.0025
*p*1w	0–1	0.5	0.420	0.010	0.5	0.1287	0.0044	0.5	0.1212	0.0041	0.5	0	
*p*II (R1)	mpdo–1				0	0.5979	0.0022		0.6055 (mpdo)			0.7011 (mpdo)	
*p*III (R2)	mpdo–1							0.5	0.6317	0.0028		0.5736 (mpdo)	
*p*IIII (R3)	mpdo–1										0.8	0.552	0.018

		EG intercalated, R_{exp} = 5.73%											
		— R_{wp} = 27.55% —			— R_{wp} = 12.39% —			— R_{wp} = 12.39% —			— R_{wp} = 26.88% —		
	Refinement limits	R0 start	R0 result	R0 σ	R1 start	R1 result	R1 σ	R2 start	R2 result	R2 σ	R3 start	R3 result	R3 σ
Repeating distances													
t smectitic (EG) (Å)	16.75–16.9	16.8	16.768	0.016	16.8	16.851	0.0050	16.8	16.8500	0.0050	16.8	16.837	0.014
Atomic occupancies													
p(Fe)	0–0.7	0.1	0.007	0.017	0.1	0.0921	0.0057	0.1	0.1004	0.0057	0.1	0.006	0.014
p(K)	0.6–1	0.8	0.6		0.8	0.658	0.0074	0.8	0.659	0.0074	0.8	0.666	0.018
p(H_2O)	0–2	0.1	2		0.1	1.75	0.032	0.1	1.73	0.032	0.1	2	
p(EG)	0.2–2	1.0	1.114	0.027	1.0	0.6924	0.0098	1.0	0.6736	0.0098	1.0	1.104	0.026
Distance to midplane													
d(Ca,H_2O) (Å)	0–2.75	2.525	2.561	0.024	2.525	2.419	0.011	2.525	2.418	0.011	2.525	2.468	0.027
d(EG) (Å)	0.434–2.75	2.15	1.513	0.015	2.15	1.457	0.014	2.15	1.443	0.014	2.15	1.492	0.017
Proportions and probabilities													
*w*I	0*–1	0.5	0.6636	0.0047	0.5	0.6820	0.0013	0.75	0.6841	0.0013	0.875	0.75	
*p*II (R1)	mpdo–1				0	0.5338	0.0027		0.5383 (mpdo)			0.6667 (mpdo)	
*p*III (R2)	mpdo–1							0.5	0.5408	0.0044		0.5 (mpdo)	
*p*IIII (R3)	mpdo–1										0.8	0.685	0.019

n.r.: Not refineable because the proportion of the corresponding component was zero. *: The lower refinement limit for R2 and R3 was increased due to the definition range.

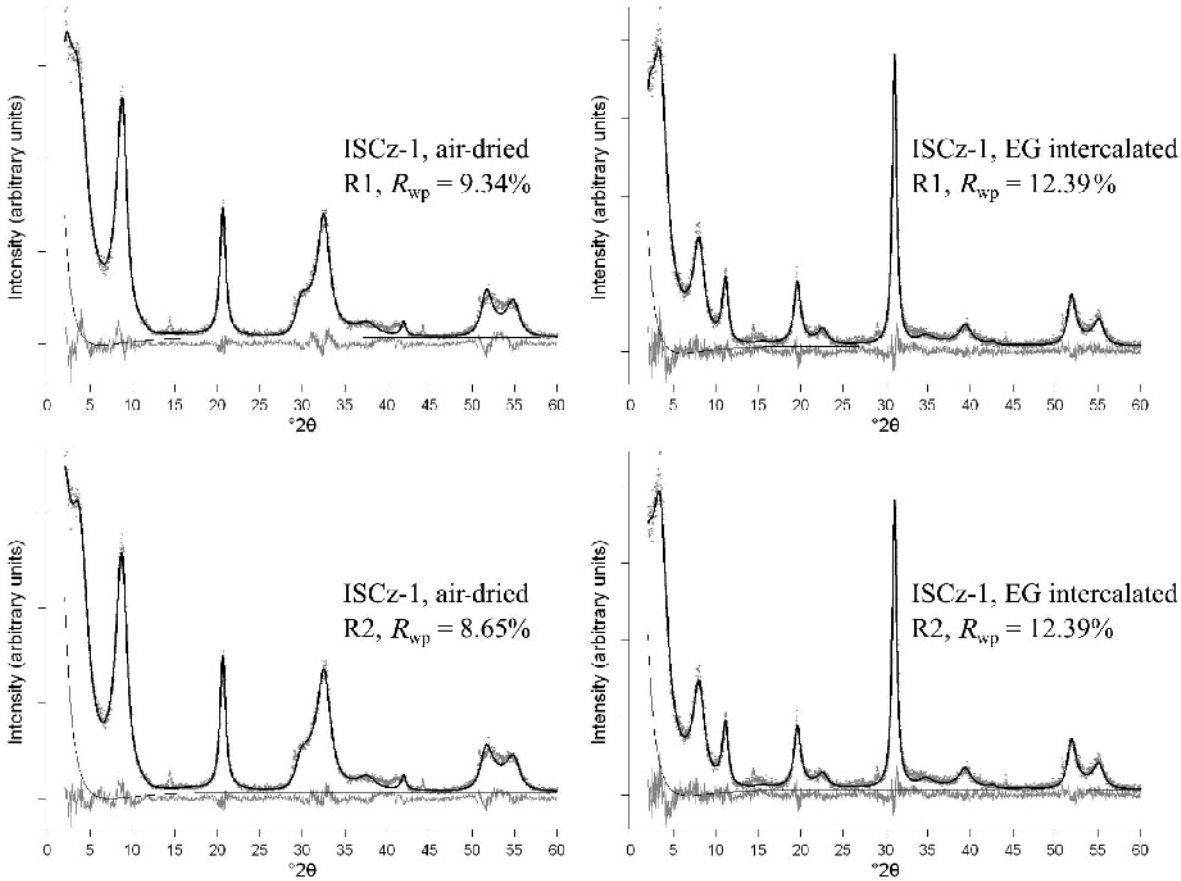

Figure 15. Refinements of sample ISCz-1 in the AD and EG states refined with the R1 and R2 models. The calculated lines of the kaolinite and corundum peaks were not shown.

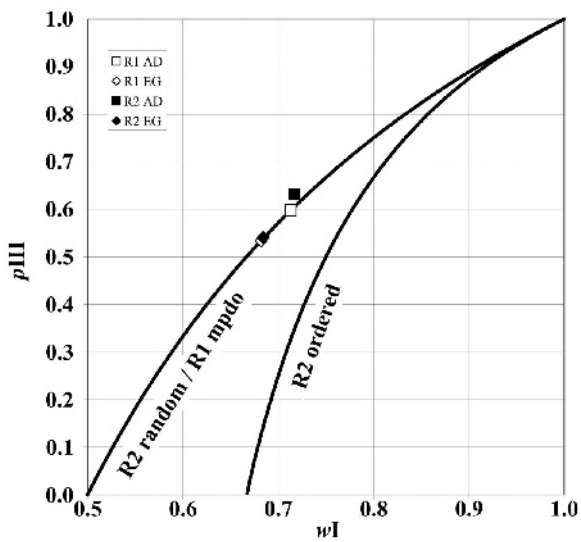

Figure 16. Refinement results of *w*I and *p*III of sample ISCz-1 with the R1 and R2 models in a junction probability diagram for R2 ordering, modified from Bethke *et al.* (1986), modified. *p*III = *p*II for the refinements with the R1 models.

solutions. The R_{wp} values of the refinements in the AD state came to 13.85% (R2) and 13.34% (R3) and those of the EG state were 16.87% (R2) and 15.45% (R3). This implies that the R3 model can be seen as the correct one to describe the stacking of this sample. The refinement in the EG state with the R2 model resulted in the case of mpdo. The two refinements with the R3 model led to *p*IIII values which plotted below the line of R3 random ordering in the junction probability diagram of R3 ordering (Figure 17). The result of the refinement in the EG state fell near or between the two lines of R3 random and R3 mpdo ordering. The gap of these two lines is much wider for the refined value of *w*I = 0.855 than for *w*I = 0.9, as in the third example of simulated data. The distinction between R2 and R3 was easier in this case. The refinement pattern of the AD state with the R2 model showed a small-intensity maximum at 5°2θ, which was not present in the measured data (Figure 18). Both models produced in the AD state a modulation in the range of 29–35°2θ which was not visible in the measured line. The peak doublet at 45°2θ could not be fitted correctly by either model. The two refinements in the EG state showed a better agreement and were

https://doi.org/10.1346/CCMN.2012.0600507 Published online by Cambridge University Press

Table 9. Refinement results of the I-S F4 sample in air-dried (AD) and EG-intercalated states. Each state was refined with four different models (R0 to R3).

		AD, R_{exp} = 3.55%											
		— R_{wp} = 24.75% —			— R_{wp} = 20.38% —			— R_{wp} = 13.85% —			— R_{wp} = 13.34% —		
	Refinement limits	R0 start	R0 result	R0 σ	R1 start	R1 result	R1 σ	R2 start	R2 result	R2 σ	R3 start	R3 result	R3 σ
Repeating distances													
t smectitic (1w) (Å)	11.65–12.85	12.5	12.85		12.5	12.85		12.5	12.85		12.5	12.85	
t smectitic (2w) (Å)	14.3–15.51	15	15.121	0.0096	15	15.047	0.0067	15	15.047	0.0067	15	15.05	0.0038
Atomic occupancies													
p(Fe)	0–0.7	0.1	0		0.1	0		0.1	0		0.1	0	
p(K)	0.6–1	0.8	0.6993	0.0084	0.8	0.6503	0.0067	0.8	0.6503	0.0067	0.8	0.7017	0.0044
p(Ca)	0.1–0.3	0.2	0.3		0.2	0.3		0.2	0.3		0.2	0.295	0.017
p(H_2O) (1w)	0–3	0.8	2.78	0.26	0.8	3		0.8	3		0.8	2.92	0.32
p(H_2O) (2w)	0–3	0.6	2.814	0.052	0.6	2.878	0.034	0.6	2.878	0.034	0.6	2.332	0.024
Distance to midplane													
d(H_2O) (Å)	1.0–1.5	1.2	1.256	0.017	1.2	1.497	0.014	1.2	1.497	0.014	1.2	1.5	
Proportions and probabilities													
*w*I	0*–1	0.5	0.8224	0.0024	0.5	0.8442	0.0013	0.75	0.8442	0.0013	0.875	0.8563	0.00070
*p*1w	0–1	0.5	0.2561	0.0087	0.5	0.2131	0.0069	0.5	0.2131	0.0069	0.5	0.1283	0.0046
*p*II (R1)	mpdo–1				0	0.8154	0.0018		0.8154 (mpdo)			0.83215 (mpdo)	
*p*III (R2)	mpdo–1							0.5	0.7970	0.0013		0.7983 (mpdo)	
*p*IIII (R3)	mpdo–1										0.8	0.7890	0.0015

		EG intercalated, R_{exp} = 7.17%											
		— R_{wp} = 23.65% —			— R_{wp} = 21.71% —			— R_{wp} = 16.87% —			— R_{wp} = 15.45% —		
	Refinement limits	R0 start	R0 result	R0 σ	R1 start	R1 result	R1 σ	R2 start	R2 result	R2 σ	R3 start	R3 result	R3 σ
Repeating distances													
t smectitic (EG) (Å)	16.75–16.9	16.8	16.75		16.8	16.764	0.0068	16.8	16.812	0.0053	16.8	16.823	0.0049
Atomic occupancies													
p(Fe)	0–0.7	0.1	0.0065	0.0067	0.1	0		0.1	0.0001	0.0045	0.1	0.0045	0.0040
p(K)	0.6–1	0.8	0.6842	0.0076	0.8	0.6753	0.0069	0.8	0.6993	0.0052	0.8	0.7136	0.0046
p(H_2O)	0–2	0.1	1.896	0.048	0.1	2		0.1	2		0.1	2	
p(EG)	0.2–2	1.0	1.070	0.014	1.0	1.093	0.013	1.0	0.8906	0.0084	1.0	0.8010	0.0068
Distance to midplane													
d(Ca,H_2O) (Å)	0–2.75	2.525	2.701	0.020	2.525	2.716	0.017	2.525	2.588	0.012	2.525	2.525	0.011
d(EG) (Å)	0.434–2.75	2.15	1.663	0.013	2.15	1.631	0.010	2.15	1.5628	0.0096	2.15	1.5202	0.0098
Proportions and probabilities													
*w*I	0*–1	0.5	0.8226	0.0020	0.5	0.8422	0.0014	0.75	0.8522	0.0008	0.875	0.8544	0.0007
*p*II (R1)	mpdo–1				0	0.8126	0.0020		0.8265 (mpdo)			0.82951 (mpdo)	
*p*III (R2)	mpdo–1							0.5	0.7903	0.0017		0.7945 (mpdo)	
*p*IIII (R3)	mpdo–1										0.8	0.7707	0.0019

n.r.: Not refineable because the proportion of the corresponding component was zero. *: The lower refinement limit for R2 and R3 was increased due to the definition range.

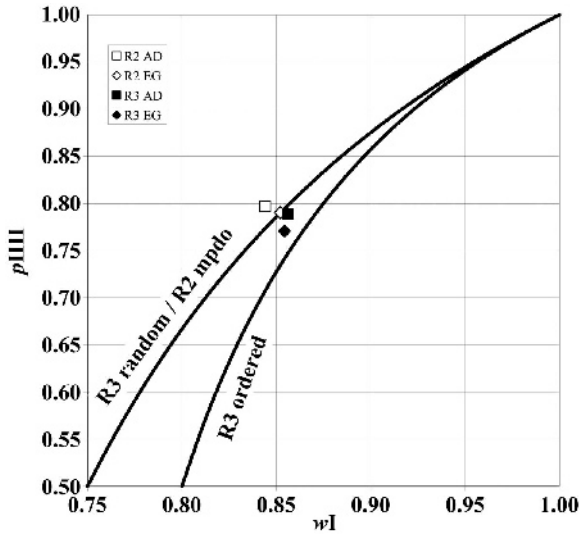

Figure 17. Refinement results of *w*I and *p*IIII of sample F4 with the R2 and R3 models in a junction probability diagram for R3 ordering, modified from Bethke *et al.* (1986). *p*IIII = *p*III for the refinements with the R2 models.

statistically more reliable if the R_{exp} value was also considered. The R_{exp} value of the two refinements in the AD state was 3.55% while that of the refinements in the EG state was 7.17%, due to the shorter counting time of the latter. The ratio of the R_{wp} to the R_{exp} value of the R3 refinement in the EG state was the most favorable. The calculated pattern of this refinement had the best agreement with the observed line. The application of the R2 model to the measurement in the EG state again showed a modulated shape below 7°2θ. The examination of the calculated pattern and the low R_{wp} value led to the result that sample F4 showed an R3 ordered stacking between random and mpdo ordering.

This sample had a low proportion of smectitic layers and the proportion of monohydrated smectitic layers was even smaller. The refinement of the related parameters failed or led to doubtful results. The refinement of t_s of the 2w state and the EG-intercalated state led to realistic results. The refined occupancies of Fe reached the lower limit for the AD state and it was refined as p(Fe) = 0.0045 for the EG state. These results were satisfactory because the occupancy of Fe calculated from the

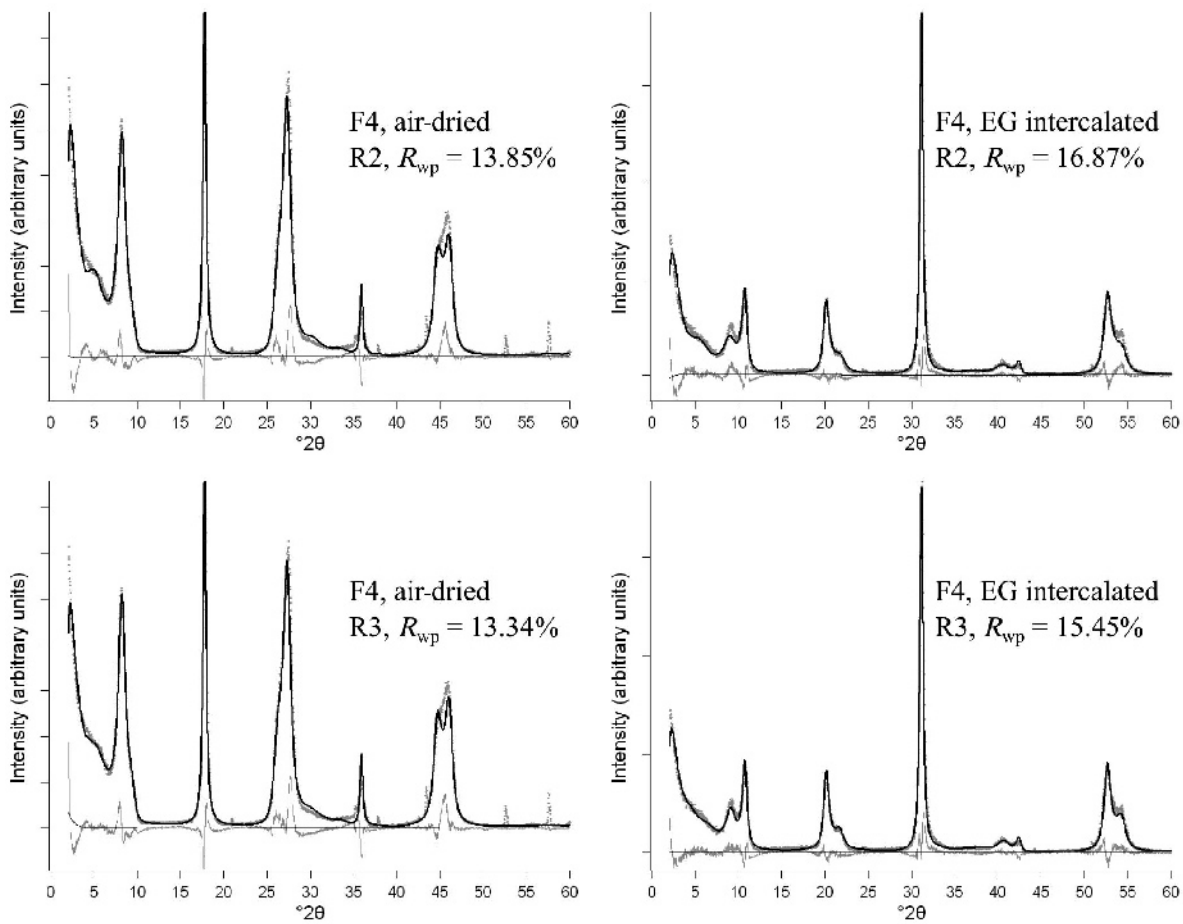

Figure 18. Refinements of sample F4 in the AD and EG states refined with the R2 and R3 models. The calculated lines of the quartz and corundum peaks were not shown.

https://doi.org/10.1346/CCMN.2012.0600507 Published online by Cambridge University Press

structural formula was quite low: $p(\mathrm{Fe})_{\mathrm{chem}} = 0.03/2 = 0.015$. The calculated occupancy of K was $p(\mathrm{K})_{\mathrm{chem}} = 0.67/w\mathrm{I} = 0.79$. The refined values of $p(\mathrm{K}) = 0.70$ (AD) and $p(\mathrm{K}) = 0.71$ (EG) were internally consistent, but differed significantly from the value calculated from the structural formula.

CONCLUSIONS

Evaluation of the refinements showed that refinement of the basal reflections of disordered stacking is possible by combining the recursive treatment of diffraction with the Rietveld method.

The nature of stacking could be identified by applying different models from R0 to R3 with intermediate starting values for the refineable parameters. A pre-adjustment of the models by introducing additional information was not necessary. Correct values could be obtained even if the starting parameters differed significantly from the optimum values. This stability allows even inexperienced users to obtain reliable results.

The uniqueness of the selection of the correct model depended on the ratio of illitic and smectitic layers. The incorrect choice of the structure model led to very high R_{wp} values for high proportions of smectitic layers. In contrast, the statistical quality of refinements with different models became comparable for high proportions of illitic layers. A detailed examination of the statistical parameters and patterns was necessary.

The inability to fit a pattern of a smectite-rich I-S with the R2 and R3 models resulted from the assumption of mpdo. High wS values were simply not allowed. The problems with determining the correct degree of R for high proportions of illitic layers is not a consequence of mpdo. The stacking probabilities of the minor component (pSS, pSSS,...) generally become small for a large amount of the other component (*e.g.* $w\mathrm{I} > 0.9$) and converge toward mpdo with increasing wI. In the extreme case of wI close to unity, the whole Reichweite concept degrades and postulating any order such as R1 or above makes no sense. This is also valid for the symmetrical (but hypothetical) case of a smectite-rich I-S with any kind of order >R0 and without mpdo.

Some types of stacking could correctly be described by two models. R0, R1 (mpdo), and R2 (mpdo) arrangements are identical to random ordering for the next higher degree of Reichweite. Stacks showing tendencies of segregation may be misinterpreted as physical mixtures.

The position-affecting parameters could be refined automatically with high accuracy. An aberration of 1% of just one of these parameters (t_{s}(1w) in the first example) increased the R_{wp} value and produced a distinct mismatch of the patterns.

Reliable occupancies and positions of cations, water, and EG molecules in smectitic interlayers were difficult to establish. Different sets of parameters produced results of statistically equal quality, even if they were definitely incorrect. For high proportions of illitic layers, the contribution of the smectitic interlayer content is simply too low. For high proportions of smectitic layers, they are strongly correlated to each other and even to the occupancies of cations in the TOT layer. In other words, the one-dimensional pattern does not contain enough information for a serious analysis of these parameters. Refinement results of Fe occupancies in smectite-dominated I-S minerals were dubious. In contrast, occupancies of K and Fe could reliably be refined for minerals with a high proportion of illite.

The observation that different sets of parameters can produce statistically equivalent results is not restricted to Rietveld refinement. This uncertainty is independent of the method used for the pattern calculation, whether fitted manually or refined automatically.

The uncertainties of the refinements of intensity-affecting parameters may become greater and the accuracy of the refinements of position-affecting parameters smaller if real measurements are analyzed. The reason here is that any crystallographic model is just an approximation of reality, while the refinement models can reflect the input models in the case of simulated data.

Nevertheless, the test of the recursive approach on real samples led to satisfactory results. The application of all four models without any additional information allowed a determination of a realistic stacking model. Parameters known from chemical analysis or from the literature could be reproduced or were at least in the same range of magnitude.

The uncertainties of the determination of the smectitic interlayer content can only be eliminated if at least a proportion of these parameters is controlled or determined by additional analysis. Multi-specimen approaches by measuring under different controlled relative humidity or intercalation treatments should guide further investigations.

Correct Rietveld modeling of basal reflections of disordered stacks, now possible for basal patterns, is needed for the refinement of powdered samples. The refinement of three-dimensional *hkl* reflections of I-S minerals for the purpose of quantitative phase analysis is demonstrated in part II (Ufer *et al*., 2012).

ACKNOWLEDGMENTS

The authors are grateful to Associate Editor, Eric Ferrage, and the reviewers, Bruno Lanson and Boris Sakharov, for useful suggestions and corrections for the manuscript.

REFERENCES

Ahn, J.H. and Buseck, P.R. (1990) Layer-stacking sequences and structural disorder in mixed-layer illite-smectite: image simulations and HRTEM imaging. *American Mineralogist*,

75, 267–275.

Aplin, A.C., Matenaar, I.F., McCarty, D.K., and van Der Pluijm, B.A. (2006) Influence of mechanical compaction and clay mineral diagenesis on the microfabric and pore-scale properties of deep-water gulf of Mexico mudstones. *Clays and Clay Minerals*, **54**, 500–514.

Bergmann, J., Friedel, P., and Kleeberg, R. (1998) BGMN – a new fundamental parameter based Rietveld program for laboratory X-ray sources, its use in quantitative analysis and structure investigations. *CPD Newsletter, Commission of Powder Diffraction, International Union of Crystallography*, **20**, 5–8.

Bethke, C.M., Vergo, N., and Altaner, S.P. (1986) Pathways of smectite illitization. *Clays and Clay Minerals*, **34**, 125–135.

Casas-Cabanas, M., Rodríguez-Carvajal, J., and Palacín, M.R. (2006) FAULTS, a new program for refinement of powder diffraction patterns from layered structures. *Zeitschrift für Kristallographie, Supplement*, **23**, 243–248.

Cheary, R.W. and Coelho, A. (1992) Fundamental parameters approach to x-ray line-profile fitting. *Journal of Applied Crystallography*, **25**, 109–121.

Dohrmann, R., Rüping, K.B., Kleber, M., Ufer, K., and Jahn, R. (2009) Variation of preferred orientation in oriented clay mounts as a result of sample preparation and composition. *Clays and Clay Minerals*, **57**, 686–694.

Drits, V.A. and Tchoubar, C. (1990) *X-ray Diffraction by Disordered Lamellar Structures.* Springer-Verlag, Berlin, Heidelberg.

Drits, V.A., McCarty, D.K., and Zviagina, B.B. (2006) Crystal-chemical factors responsible for the distribution of octahedral cations over trans- and cis-sites in dioctahedral 2:1 layer silicates. *Clays and Clay Minerals*, **54**, 131–152.

Ferrage, E., Lanson, B., Sakharov, B.A., and Drits, V.A. (2005a) Investigation of smectite hydration properties by modeling experimental X-ray diffraction patterns: Part I. Montmorillonite hydration properties. *American Mineralogist*, **90**, 1358–1374.

Ferrage, E., Lanson, B., Malikova, N., Plançon, A., Sakharov, B.A., and Drits, V.A. (2005b) New Insights on the Distribution of Interlayer Water in Bi-Hydrated Smectite from X-ray Diffraction Profile Modeling of 00l Reflections. *Chemistry of Materials*, **17**, 3499–3512.

Ferrage, E., Lanson, B., Sakharov, B.A., Geoffroy, N., Jacquot, E., and Drits, V.A. (2007) Investigation of dioctahedral smectite hydration properties by modeling of X-ray diffraction profiles: Influence of layer charge and charge location. *American Mineralogist*, **92**, 1731–1743.

Gailhanou, H., van Miltenburg, J.C., Rogez, J., Olives, J., Amouric, M., Gaucher, E.C., and Blanc, P. (2007) Thermodynamic properties of anhydrous smectite MX-80, illite IMt-2 and mixed-layer illite-smectite ISCz-1 as determined by calorimetric methods. Part I: Heat capacities, heat contents and entropies. *Geochimica et Cosmochimica Acta*, **71**, 5463–5473.

Gualtieri, A.F., Ferrari, S., Leoni, M., Grathoff, G., Hugo, R., Shatnawi, M., Paglia, G., and Billinge, S. (2008) Structural characterization of the clay mineral illite-1M. *Journal of Applied Crystallography*, **41**, 402–415.

Howard, S.A. and Preston, K.D. (1989) Profile fitting of powder diffraction patterns. Pp. 217–275 in: *Modern Powder Diffraction* (D.L. Bish and J.E. Post, editors). Reviews in Mineralogy, **20**, Mineralogical Society of America, Washington, D.C.

Jagodzinski, H. (1949) Eindimensionale Fehlordnung in Kristallen und ihr Einfluss auf die Röntgeninterferenzen. I. Berechnung des Fehlordnungsgrades aus den Röntgenintensitäten. *Acta Crystallographica*, **2**, 201–207.

Leoni, M., Gualtieri, A.F., and Roveri, N. (2004) Simultaneous refinement of structure and microstructure of layered materials. *Journal of Applied Crystallography*, **37**, 166–173.

Maegdefrau, E. and Hofmann, U. (1937) Glimmerartige Mineralien als Tonsubstanzen. *Zeitschrift für Kristallographie*, **98**, 31–59.

Marshall, C.E. (1935) Layer lattices and the base exchange clays. *Zeitschrift für Kristallographie*. **91**, 443–449.

Marshall, C.E. (1949) *The Colloid Chemistry of the Silicate Minerals*. Academic Press, New York.

Oie, T., Topol, I.A., and Burt, S.K. (1994) Ab initio and density functional calculations on ethylene glycol. *Journal of Physical Chemistry*, **98**, 1121–1128.

Plançon, A. (2004) Consistent modeling of the XRD patterns of mixed-layer phyllosilicates. *Clays and Clay Minerals*, **52**, 47–54.

Plançon, A. and Drits, V.A. (2000) Phase analysis of clays using an expert system and calculation programs for X-ray diffraction by two-and three-component mixed-layer minerals. *Clays and Clay Minerals*, **48**, 57–62.

Plançon, A. and Roux, J. (2010) Software for the assisted determination of the structural parameters of mixed-layer phyllosilicates. *European Journal of Mineralogy*, **22**, 733–740.

Reynolds, R.C., Jr. (1980) Interstratified clay minerals: Pp. 249–303 in: *Crystal Structures of Clay Minerals and their X-ray Identification* (G.W. Brindley and G. Brown, editors). Mineralogical Society, London.

Reynolds, R.C., Jr. (1985) *NEWMOD: a computer program for calculation of one-dimensional diffraction patterns of mixed-layer clays*. R.C. Reynolds, 9 Brook Rd., New Hampshire 03755, USA.

Ross, C.S. and Hendricks, S.B. (1945) Minerals of the montmorillonite group, their origin and relation to soils and clays. U.S. Geological Survey, Professional Paper **205-B**, pp. 23–79.

Sakharov, B.A., Besson, G., Drits, V.A., Kameneva, M.Y., Salyn, A.L., and Smoliar, B.B. (1990) X-ray study of the nature of stacking faults in the structure of glauconites. *Clay Minerals*, **25**, 419–435.

Sakharov, B.A., Lindgreen, H., Salyn, A.L., and Drits, V.A. (1999) Determination of illite-smectite structures using multispecimen X-ray diffraction profile fitting. *Clays and Clay Minerals*, **47**, 555–566.

Środoń, J., Elsass, F., McHardy, W.J., and Morgan, D.J. (1992) Chemistry of illite-smectite inferred from TEM measurements of fundamental particles. *Clay Minerals*, **27**, 137–158.

Taylor, R.M. and Norrish, K. (1966) The measurement of orientation distribution and its application to quantitative X-ray diffraction analysis. *Clay Minerals*, **6**, 127–142.

Treacy, M.M., Newsam, J.M., and Deem, M.W. (1991) A General Recursion Method for Calculating Diffracted Intensities From Crystals Containing Planar Faults. *Proceedings of the Royal Society of London*, **A433**, 499–520.

Treacy, M.M., Newsam, J.M., and Deem, M.W. (1993) Simulation of electron diffraction patterns from partially ordered layer lattices. *Ultramicroscopy*, **52**, 512–522.

Ufer, K., Roth, G., Kleeberg, R., Stanjek, H., and Dohrmann, R. (2004) Description of X-ray powder pattern of turbostratically disordered layer structures with a Rietveld compatible approach. *Zeitschrift für Kristallographie*, **219**, 519–527.

Ufer, K., Kleeberg, R., Bergmann, J., Curtius, H., and Dohrmann, R. (2008) Refining real structure parameters of disordered layer structures within the Rietveld method. *Zeitschrift für Kristallographie Supplements*, **27**, 151–158.

Ufer, K., Kleeberg, R., Bergmann, J., and Dohrmann, R. (2012) Rietveld refinement of disordered illite-smectite mixed

https://doi.org/10.1346/CCMN.2012.0600507 Published online by Cambridge University Press

layer structures by a recursive algorithm. Part II: Powder pattern refinement and quantitative phase analysis. *Clays and Clay Minerals*, **60**, 536–553.

Yuan, H. and Bish, D.L. (2010a) NEWMOD+ , a new version of the NEWMOD program for interpreting X-ray powder diffraction patterns from interstratified clay minerals. *Clays and Clay Minerals*, **58**, 318–326.

Yuan, H. and Bish, D.L. (2010b) Automated fitting of X-ray powder diffraction patterns from interstratified phyllosilicates. *Clays and Clay Minerals*, **58**, 727–742.

(*Received 14 September 2011; revised 24 August 2012; Ms. 615; AE: E. Ferrage*)